Slit2 is essential for correct retinal ganglion cell axon fasciculation and midline crossing in the zebrafish

Running title: Slit2 in retinal axons fasciculation

Authors: Camila Davison and Flavio R. Zolessi

Affiliation: Sección Biología Celular, Facultad de Ciencias, Universidad de la República, Iguá 4225, 11400 Montevideo; Institut Pasteur de Montevideo, Mataojo 2020, 11400 Montevideo. Uruguay.

Corresponding author: F.R.Z., fzolessi@fcien.edu.uy

Author's contributions: CD designed and performed the experimental manipulations, analyzed the data and wrote the manuscript; FRZ directed the research, designed part of the experiments, analyzed part of the data and wrote the manuscript.

Acknowledgements: The authors thank William A. Harris, University of Cambridge, and José L. Badano, Institut Pasteur de Montevideo, for continued support with lab space and materials, as well as fruitful discussion; Uriel Koziol and Matías Preza, Biología Celular, Facultad de Ciencias, UdelaR, for help with whole-mount fluorescent *in situ* hybridization; Juan Pablo Fernández, Yale University, for invaluable help and discussion on CRISPR-Cas9 technique; Kristen Kwan for providing plasmids; Casandra Carrillo and Gisell González, Zebrafish Lab, Institut Pasteur de Montevideo, for fish maintenance and care; Marcela Díaz and Tabaré De Los Campos, Microscopy Unit, Institut Pasteur de Montevideo, for technical assistance on microscopy. This work was partly funded by an ANII-FCE grant to FRZ (1_1_2014_1_4982); CAP-UdelaR Master and PhD fellowships to CD; FOCEM-Institut Pasteur de Montevideo Grant (COF 03/11); Programa de Desarrollo de las Ciencias Básicas (PEDECIBA, Uruguay).

Conflict of interest: The authors declare no conflict of interest.

Data availabilty statement: The data that support the findings of this study, as well as original materials, are available from the corresponding author upon reasonable request.

ABSTRACT

The functional connection of the retina with the brain implies the extension of retinal ganglion cells axons through a long and tortuous path. Slit-Robo signaling has been implicated in axon growth and guidance in several steps of this journey. Here, we analyzed in detail the expression pattern of *slit2* in zebrafish embryos by whole-mount fluorescent *in situ* hybridization, to extend previous work on this and other species. Major sites of expression are amacrine cells in the retina from 40 hpf, as well as earlier expression around the future optic nerve, anterior to the optic chiasm, two prominent cell groups in the anterior forebrain and the ventral midline of the caudal brain and spinal cord. To further characterize *slit2* function in retinal axon growth and guidance, we generated and phenotypically characterized a null mutant for this gene, using CRISPR-Cas9 technology. Although no evident defects were found on intraretinal axon growth or in the formation of the optic tracts or tectal innervation, we observed very characteristic and robust impairment on axon fasciculation at the optic nerves and chiasm. The optic nerves appeared thicker and defasciculated only in maternal-zygotic mutants, while a very particular unilateral nerve-splitting phenotype was evident at the optic chiasm in a good proportion of both zygotic and maternal-zygotic mutants. Our results support the idea of a channeling role for Slit molecules in retinal ganglion cell axons at the optic nerve level, in addition to a function in the segregation of axons coming from each nerve at the optic chiasm.

KEYWORDS

Visual pathway; optic nerve; optic chiasm; CRISPR-Cas9; axon guidance

1 - INTRODUCTION

The neural retina of vertebrates develops as an evaginated extension of the early forebrain, to which it remains connected through the optic stalk. Hence, the axons of its projection neurons, the retinal ganglion cells (RGCs), must undergo a long and highly regulated process of guided growth to eventually reach their synaptic targets in the mesencephalic roof. RGCs differentiate in the basal-most cell layer of the retina, and grow an axon from their basal poles, to later develop a dendritic tree from the apical region (Zolessi et al., 2006). Along their journey, RGC growth cones encounter several different signaling molecules that guide their path (Herrera et al., 2019). The first portion is particularly challenging, as it includes intraretinal guidance to find the optic nerve exit, the turning and fasciculation to form the optic nerve, the exit from the eye and growth along the optic stalk, and crossing (or not, depending on species) at the optic chiasm. A family of signaling molecules, the Slit proteins, and their Robo receptors, have been found to be relevant in these events, largely acting as repulsive factors, although their exact mechanisms of action are still not completely understood (Herrera et al., 2019).

Slit molecules constitute a family of secreted glycoproteins of ≈200 kDa, with various forms present across animals with bilateral symmetry (Brose and Tessier-Lavigne, 2000). Invertebrates like *D. melanogaster* have only one form of this protein (named Slit), while there are three in most vertebrates (Slit1-3) and four in the zebrafish (Slit1a, 1b, 2 and 3) (Yeo et al., 2001; Hutson et al., 2003). These proteins consist of five major regions: one N-terminal signal peptide, four stretches of leucine-rich repeat (LRR) domains (also called D1-D4) in tandem with disulfide bonds, seven to nine epidermal growth factor-like (EGF-like) repeats, an Agrin-Perlecan-Laminin-Slit (ALPS)/Laminin-G-like domain, and a C-terminal cysteine knot (Blockus and Chédotal, 2016). Some Slit proteins can be cleaved by proteolytic enzymes between the fifth and sixth EGF-like domains to generate a long N-terminal Slit segment (SlitN) and a short C-terminal Slit segment (SlitC) (Nguyen Ba-Charvet et al., 2001). Although Slit ligands are secreted, their diffusion is limited due to their strong association with extracellular matrix components such as collagen IV and dystroglycan (Xiao et al., 2011; Wright et al., 2012).

Slit main receptors are the Robo family of proteins, to which they bind through the second LRR domain (Howitt et al., 2004). There are four genes coding for these receptors in vertebrates, including the zebrafish (Robo1-4) (Lee et al., 2001; Park et al., 2003). No enzymatic activity has been attributed to the Robo receptors, and the intracellular signaling seems to be propagated mainly through cytoplasmic kinases, and the actin and microtubule cytoskeleton (Blockus and Chédotal, 2016). Increasing evidence suggests that Slits bind to other molecules, receptors or coreceptors. Heparan sulfate proteoglycan (HSP) binds to both Slit and Robo to form a ternary complex to stabilize their interaction at the membrane (Steigemann et al., 2004), while two Slit2 proteins can bind to each other at the fourth LRR domain to form homodimers (Seiradake et al., 2009). The C-terminal fragment of Slit2 (Slit2C), previously thought to be inactive, has recently been shown to act through PlexinA1, a Semaphorin receptor, to mediate axon repulsion (Delloye-Bourgeois et al., 2015).

In the zebrafish, *slit2* expression has been found within the optic stalk and surrounding the optic nerve where RGC axons enter the brain, as well as in the retina (Chalasani et al., 2007). Furthermore, in the ventral forebrain, *slit2* is expressed in the rostral margin of the optic recess, which is located midway between the anterior commissure and post-optic commissure, and in close proximity to the optic chiasm (Hutson and Chien, 2002). In tissue culture, Slit2 acts as a chemorepellent and collapsing factor for retinal axons (Erskine et al., 2000; Niclou et al., 2000), function that also helps it guide these axons *in vivo* (Ringstedt et al., 2000). Slit2 was shown to be important for intraretinal axon pathfinding in mice (Thompson et al., 2006), and to act together with Slit1 to channel RGC axons to their correct location at the optic chiasm (Plump et al., 2002). Paradoxically, in addition to its repulsive activity, Slit2 also appears to have axon-branching and outgrowth-promoting activity in some contexts (Wang et al., 1999). Finally, it also plays a role in dendritic development. For example, roles in self-avoidance during Purkinje cells dendritic development (Gibson et al., 2014), and in the promotion of dendrite branching in *Xenopus* RGCs *in vitro* (Hocking et al., 2010) have been demonstrated.

Here, we describe a new *slit2* mutant in the zebrafish (NM_131753.1:g.30_39del), generated through CRISPR-Cas9, and present an initial characterization of its phenotype

regarding RGCs and their axons. In addition to a mild effect on the thickness of the retinal inner plexiform layer, we found that Slit2 is important for RGC axon fasciculation at the optic nerve and crossing at the optic chiasm, while having no apparent function in axon sorting at the optic tract and optic tectum.

2- MATERIALS AND METHODS

2.1 - Fish breeding and care

Zebrafish were maintained and bred in a stand-alone system (Tecniplast, Buguggiate, Italy), with controlled temperature (28 °C), conductivity (500 µS/cm2) and pH (7.5), under live and pellet dietary regime. Embryos were raised at temperatures ranging from 28.5 to 32 °C and staged in hours post-fertilization (hpf) according to Kimmel and collaborators (Kimmel et al., 1995). We used wild-type (Tab5), SoFa1 triple transgenic (*atoh7*:gap-RFP/ptf1a:cytGFP/*crx*:gap-CFP; Almeida et al., 2014) and the CRISPR-generated mutant line NM_131753.1:g.30_39del (hereafter denoted as *slit2-/-*). All the manipulations were carried out following the approved local regulations (CEUA-Institut Pasteur de Montevideo, and CNEA).

2.2 - Generation of the *slit2-/-* line

We designed four single-guide RNAs (sgRNA) against the *slit2* gene using the CRISPRscan tool (Moreno-Mateos et al., 2015; Supplementary Table 1). We then tested them individually by injecting each one together with mRNA for zfCas9 flanked by two nuclear localization signal sequences (nCas9n; Jao et al., 2013). One of them, complementary to a sequence in the first exon of the coding sequence (sgRNA *slit2* 21; Supplementary Table 1), presented no toxic effects and was highly efficient, as evidenced by agarose gel electrophoresis. We injected one-cell stage Tab5 embryos with this sgRNA, together with Cas9 mRNA, and raised them to adulthood. A chosen female was subjected to outcross with a wild-type male, and the progeny was genotyped at 48 hpf. After gel

electrophoresis and sequencing, we found a set of four different mutations. The embryos obtained from the outcross were raised to adulthood, and were then selected for the desired 10 base pair deletion through fin clipping. This gave rise to the heterozygous line, which was crossed to obtain the *slit2-/-* mutant.

2.3 - Morpholino treatment

The morpholino oligomers (MOs) used in this study were obtained from Gene Tools (Philomath, USA). The *slit2* MO has been previously used to target zebrafish *slit2* translational initiation: *slit2*-ATG (Supplementary Table 1; Barresi et al., 2005). For *ptf1a* knock-down, a combination of two MOs was used: a translation blocking *ptf1a* MO1 and a splice-blocking *ptf1a* MO2 (Supplementary Table 1; Almeida et al., 2014). 1.5 ng of the *slit2*MO or, alternatively, a mix of 2 ng each of the *ptf1a* MO1+MO2 were injected in the yolk of 1–4 cell-stage embryos, at a maximum volume of 2 nL. As control, we used matching doses of a standard control MO (Supplementary Table 1) from Gene Tools (Philomath, USA).

2.4 - Whole-mount immunofluorescence

Embryos were grown in 0.003 % phenylthiourea (Sigma, St. Louis, USA) from 10 hpf onwards to delay pigmentation, and fixed overnight at 4 °C, by immersion in 4 % paraformaldehyde in phosphate buffer saline, pH 7.4 (PFA-PBS). For whole-mount immunostaining all subsequent washes were performed in PBS containing 1 % Triton X-100. Further permeability was achieved by incubating the embryos in 0.25 % trypsin-EDTA for 10–15 min at 0 °C. Blocking was for 30 min in 0.1 % bovine serum albumin (BSA), 1 % Triton X-100 in PBS. The primary antibodies, diluted in the blocking solution, were used as follows: zn8 (ZIRC, Oregon, USA), recognizing the adhesion molecule neurolin/DM-grasp, 1/100; anti-acetylated α-tubulin (Sigma, St. Louis, USA), 1/1000; anti-neurofilament-associated antigen (3A10, DSHB), 1/100. The secondary antibody used was anti-mouse IgG-Alexa 488 (Life Technologies, Carlsbad, USA), 1/1000. When necessary, TRITC-conjugated phalloidin (Sigma, St. Louis, USA) was mixed with the

secondary antibody. Nuclei were fluorescently counterstained with methyl green (Prieto et al., 2014). All antibody incubations were performed overnight at 4 °C. Embryos were mounted in 1.5 % agarose-50 % glycerol in 20 mM Tris buffer (pH 8.0) and stored at 4 °C or −20 °C. Observation of whole embryos was performed using a Zeiss LSM 880 laser confocal microscope, with a 25x 0.8 NA glycerol immersion objective.

2.5 - Cryosections

Five-day-old embryos were fixed as described above, washed in PBS and cryoprotected by a 30 min incubation in 5% sucrose in PBS, followed by a 45 min incubation in 20% sucrose in PBS. The embryos were then left overnight in a mixture of 15% sucrose and 7.5% gelatin in PBS at 39 °C. The blocks were made in the same gelatin-sucrose solution the next day. Transverse cryosections (20 µm) were made on a Reichert-Jung Cryocut E cryostat and adhered to positive charged slides. On the next day, the gelatin was removed through a 30 min incubation at 39 °C in PBS, and three subsequent PBS washes at room temperature. After labeling, mounting was made using 70% glycerol in 20 mM Tris buffer (pH 8.0). Observation was performed using a Zeiss LSM 880 laser confocal microscope, with a 63x 1.4 NA oil immersion objective.

2.6 - Whole-mount fluorescent *in situ* hybridization

Phenylthiourea-treated embryos were fixed at 48 hpf in PFA-PBS as described, transferred to 100% methanol on the next day, and kept at -20 °C until further use. We performed whole-mount fluorescent in situ hybridization (WM-FISH) using digoxigenin-labeled probes, following the protocol described by Koziol et al. (2014). The *slit2* probe was obtained from the pSPORT1-slit2 plasmid, kindly provided by Kristen Kwan and originally generated by Yeo et al. (Yeo et al., 2001). Through PCR, we obtained an 897 bp probe complementary to the 3' region of the mRNA. The sequences for the primers used are shown in Supplementary Table 1.

2.7 - Lipophilic dye labeling

Phenylthiourea-treated embryos were fixed at 48 hpf or 5 dpf as described above. They were then immobilized on glass slides using agarose and injected with 1,1'-dioctadecyl-3,3,3',3'-tetramethylindocarbocyanine perchlorate (DiI, Molecular Probes) or 3,3'-dioctadecyloxacarbocyanine perchlorate (DiO, Molecular Probes) dissolved in chloroform. For optic chiasm observation, DiI was injected into the vitreous chamber of one eye in 48 hpf embryos, whereas DiO was injected into the contralateral eye. For optic tectum observation, DiI was injected either in the ventral or the temporal region of the retina of 5 dpf larvae, at the level of the inner plexiform layer. DiO, on the other hand, was injected either in the dorsal or the nasal region of the retina, respectively. In all of the cases, after the injection the embryos or larvae were incubated for 48 hours at room temperature and mounted in agarose-glycerol.

2.8 - Data analysis

Images were analyzed using Fiji (Schindelin et al., 2012). Optic nerve diameter was measured manually on maximum intensity z-projections of the confocal stacks. Plot profiles were built from a transect spanning the nerve, and the diameter was measured at 50% of the peak intensity. For optic tract thickness and dorsal/ventral retinotopic segregation analysis, plot profiles were built from a transect drawn on maximum intensity z-projections from DiI/DiO-labeled samples. Whole retina, ganglion cell layer and inner plexiform layer thickness were measured manually on a single confocal plane perpendicular to the retina. Volume measurements (whole retina and zn8-positive region) were performed and analyzed using intensity-based thresholding aided by manual selection as previously described (Lepanto et al., 2016).

All statistical analysis was performed using GraphPad Prism software. As a routine, the data sets were checked for normality using Shapiro-Wilk normality test. In the case of normal data, we performed a Student's *t*-test for mean comparison.

3 - RESULTS

3.1 - *slit2* mRNA is expressed near RGCs and their axons in the retina and proximal visual pathway

In order to assess the expression pattern of *slit2* in more detail, we used whole-mount fluorescent *in situ* hybridization (WM-FISH). We focused on key stages in RGC differentiation in the zebrafish, namely 24, 32, 40, 48 and 72 hpf. No signal was detected in the retina at either 24 or 32 hpf, although a strong signal was observed along the floor plate and in different cell clusters, particularly at 30 hpf (Supplementary Fig. 1). The earliest signal in the retina was evident at 40 hpf, at the ciliary marginal zone (CMZ) and in a small group of cells at the innermost portion of the forming inner nuclear layer (Fig. 1a,b; Supplementary Video 1). Their position and general morphology indicate they might be a subset of amacrine cells. Signal at the CMZ disappeared by 48 hpf, while expression in these inner nuclear layer cells became progressively stronger from this stage (Fig. 1c,d; Supplementary Video 2) to 72 hpf (Fig. 1f,g; Supplementary Video 3). To determine the identity of these *slit2*-expressing cells, we depleted amacrine cells using a combination of two morpholino oligomers directed to the transcription factor Ptf1a, previously shown to be effective for this purpose (Fig. 1h; Almeida et al., 2014). In these embryos, *slit2* expression in the retina disappeared (Fig. 1i), while signal was still evident in other regions, such as the floor plate (Supplementary Fig. 2). Hence, the *slit2*-expressing cells in the retina are indeed a subset of amacrine cells located at the inner nuclear layer.

From 40 hpf, *slit2* expression was also evident all along the optic nerve area, inside and outside the retina (Fig. 2a; Supplementary Video 4), and by 48 hpf, expression was detected in cells surrounding the extra-retinal optic nerves, as has been previously described (Fig. 2b; Supplementary Video 5; Chalasani et al., 2007), and in a few easily-individualized cells on the anterior side of the optic tract (Fig. 2c; Supplementary Video 5). In addition, we observed a strong signal in two round, bilateral structures at the ventral portion of the forebrain (also described in Chalasani et al., 2007), detectable from 30 hpf, and strongly labeled by 40 hpf (Fig. 2a; Supplementary Figure 1;

Supplementary Video 4). At 72 hpf, no expression was detected at the optic chiasm or the optic tectum, as previously reported (Fig. 2d,e).

3.2 - A zebrafish null mutant for *slit2* is viable and presents no visible external phenotype

To investigate the function of Slit2 *in vivo*, we used the CRISPR/Cas9 technology to generate a zebrafish strain harboring a mutation in the *slit2* locus. For this purpose, we designed four single guide RNAs (sgRNAs) and tested their efficiency by microinjection in wild-type embryos (Supplementary Table 1). The sgRNA "*slit2* 21" proved to be highly efficient and showed no toxicity, and was therefore chosen for further experiments. F0 mosaic individuals were outcrossed with wild-type adults, which revealed the presence of a limited number of mutations in the germline, usually around four or five. We then selected a female from the F0 which harbored four different mutations in the germline (Supplementary Table 2), and F1 adults were generated by outcross with a wild-type male. These adults were genotyped and the mutation we selected to maintain and further analyze consists of a 10 base-pair deletion in exon 1, which causes a frameshift that leads to a protein truncation before the first LRR domain (Fig. 3a-c; Supplementary Fig. 3). As a consequence, this allele is expected to behave as a functional null. The homozygous individuals are viable and fertile, which allowed us to maintain both heterozygous and homozygous adult fish. We assessed the phenotype by incrossing either heterozygous (obtaining *slit2+/+* wild-types, *slit2+/-* heterozygous and *slit2-/-* zygotic mutant embryos) or homozygous adults (obtaining maternal-zygotic mutants, from now on denoted as *slit2-/-*^{mz}). The *slit2+/-*, *slit2-/-* and *slit2-/-*^{mz} were externally indistinguishable from wild-type embryos, as was the case for *slit2* morpholino-treated embryos (Fig. 3d).

3.3 - *slit2* mutants present a thicker retinal inner plexiform layer

The fact that *slit2* is expressed by amacrine cells suggested it might play a role in either RGC differentiation or the formation of the inner plexiform layer, where bipolar axons

establish synapses with RGC and amacrine cells dendrites. We set out to determine if that was the case by looking at 5 dpf larvae, where retinal lamination and RGC dendritic development is mostly complete. F-actin and nuclei labeling of mutant larvae revealed that the overall structure and organization of the retina was not affected (Fig. 4a). Moreover, the formation of sub-laminae in the inner plexiform layer did not seem to be impaired. We proceeded to measure ganglion cell layer and inner plexiform layer thickness relative to the total thickness of the neural retina, and found that, while ganglion cell layer size was not affected in either *slit2+/-*, *slit2-/-* or *slit2-/-*^{mz} larvae, the inner plexiform layer was slightly, but significantly thicker in *slit2 -/-* and *slit2-/-*^{mz}, but not in *slit2+/-* larvae (Fig. 4b-d). In no case did RGC immunostaining using the anti-neurolin antibody zn8 reveal detectable defects on RGC morphology or axon growth inside the retina, as evidenced at 48 hpf (Supplementary Fig. 4a). In addition, in these zn8-labeled embryos, there were no significant differences in the volume of the ganglion cell layer between wild-type and maternal-zygotic mutants, indicating that the observed increase in IPL thickness cannot be explained by an increase in the number of RGCs (Supplementary Fig. 4b).

3.4 - Slit2 is important for RGC axon fasciculation in the extra-retinal optic nerve

The effect of the mutation of *slit2* on RGC axon growth and guidance was assessed on 48 hpf embryos. As a first observation, zn8 labeling showed that these axons are able to form an apparently normal optic fiber layer in the retina, an optic nerve exit and extra-retinal optic nerve (Fig. 5a,b; Supplementary Fig. 4a). Axons also apparently crossed at the optic chiasm to extend along contralateral optic tracts. One of the most conspicuous defects was evident only in *slit2-/-*^{mz} embryos, which presented thicker extra-retinal optic nerves at the region proximal to the nerve exit (Fig. 5b). This phenotype was not observed in *slit2+/-* or *slit2-/-* embryos (Fig. 5a). The increase in nerve thickness was accompanied by a lower intensity in zn8 labeling, and, at higher magnifications, it was possible to observe that axons or thin axon bundles appeared relatively separated (Fig. 5b). These observations were further confirmed by a fluorescence intensity profile across wild-type and *slit2-/-*^{mz} nerves (Fig. 5d). We also quantitatively analyzed the

difference in thickness between all the conditions, including MO treatment, both for the intra- and the extra-retinal portions of the optic nerve. No difference in thickness was found for intra-retinal optic nerves between mutant or morphant and wild-type embryos (Fig. 5e). A significantly thicker extra-retinal optic nerve was however evident in *slit2-/-*^{mz}. In the case of the *slit2* morpholino treatment, a wider data dispersion in optic nerve thickness, with no significant difference to control, was observed (Fig. 5e).

We also found what appear to be fasciculation defects in a different subset of commissural axons, namely those that form the anterior commissure (AC) in the telencephalon (Supplementary Fig. 5). Axon labeling with anti-acetylated tubulin antibody revealed a thicker tract of the AC in *slit2-/-*^{mz} embryos, as well as some misguided axons. This phenotype was evident from 30 hpf and became more prominent by 40 hpf. Similar defects were not observed in the post-optic commissure (POC) tract.

3.5 - Slit2 is important for RGC axon organization at the optic chiasm

In several cases, zn8 labeling revealed a second defect in the optic nerve of mutant embryos, at the level of the optic chiasm (arrowhead in Fig. 5a; Supplementary Video 6). To better characterize this observation, we differentially labelled the optic nerves using the lipophilic dyes DiI and DiO (Fig. 6). In *slit2+/+* embryos, all the axons belonging to one of the nerves crossed rostrally (and slightly ventral) to the axons from the contralateral nerve (Fig. 6a; Supplementary Video 7), as has been previously described (Macdonald et al., 1997). In *slit2-/-* and *slit2-/-*^{mz} embryos, as well as in *slit2* morphants, on the other hand, one optic nerve frequently split into two groups of axons that surrounded the contralateral nerve (Fig. 6a, b; Supplementary Video 8). Surprisingly, this phenotype was observed with a higher frequency in *slit2-/-* mutant embryos than in *slit2-/-*^{mz} mutants and *slit2* morphants, as assessed by zn8 labeling (Fig. 6d). Moreover, *slit2+/-* embryos also presented crossing defects, albeit with lower frequency (Fig. 6d). When considering which eye the nerve that split came from, we found that the proportion between left and right eye came close to 1:1 for all cases (Fig. 6e). This is comparable to wild-type embryos, where we found the same proportion when assessing which nerve crossed rostrally/dorsally with respect to the other (Fig. 6e). In no case did

we observe ipsilateral crossing of axons. Midline crossing defects were not found in axons from another example of commissural neurons, Mauthner cells (Supplementary Fig. 6).

3.6 - Slit2 is not important for axon sorting at the optic tract and optic tectum

Given the crossing defects found in *slit2* mutant and morphant embryos at the optic chiasm, we wondered if the lack of Slit2 would affect axon topographic sorting at the optic tract and the optic tectum. This can be visualized in fixed whole-mount zebrafish larvae by injection of the lipophilic dyes DiI and DiO in the dorsal (D) and ventral (V), or nasal (N) and temporal (T) quadrants of the retina (Fig. 7; Baier et al., 1996). After contralateral eye removal, the corresponding axonal projections in the optic tract can then be analyzed in lateral or dorsal view. Axon sorting at the optic tract was not affected in *slit2-/-^{mz}* larvae (Fig. 7a). Fluorescent intensity plots show that DiI- and DiO-labeled axons remained spatially separated along the optic tract in dorsoventral labeling (Fig. 7b). Similarly, axon sorting at the optic tectum in *slit2-/-^{mz}* and *slit2* morphant embryos did not show visible defects when compared to wild-type/control embryos, in neither of the labeling strategies (Fig. 7c).

4 - DISCUSSION

Despite the many previous reports on the role of the Slit-Robo pathway in RGCs axon growth and guidance, some of them mentioned in the Introduction, information on the function of Slit2 in the zebrafish RGCs has been fragmentary, partly due to the absence of a characterized mutant line. Here, we describe the generation of a null mutation in the zebrafish *slit2* locus, using CRISPR-Cas9 genome editing technology, and its primary characterization by studying the elicited phenotype on RGCs and their axons, inside and outside the retina.

Although we did not find RGC axon guidance defects inside of the retinal tissue in our mutant or morpholino analyses, like described for mouse mutants (Thompson et al.,

2006, 2009), we did observe a slight thickening of the inner plexiform layer in *slit2-/-* and *slit2-/-^{mz}* larvae, a phenomenon that could be due to different factors. In the first place, the inner plexiform layer is where RGC dendrites are localized. Different functions in dendrite development, including growth promotion, have been reported for Slit signaling (see for example Whitford et al., 2002; Gibson et al., 2014). In the particular case of cultured *Xenopus* RGCs, Slit2 was found to promote dendrite branching, but not growth (Hocking et al., 2010).

A function for Slit2 in zebrafish RGC dendrite development also seems likely when considering the strong *slit2* expression we observed in amacrine cells. This expression is maximal at around 48-72 hpf, a developmental stage when dendritic trees are developing (Choi et al., 2010). It is important to note that *slit2* was only expressed by amacrine cells localized in the inner nuclear layer and not by displaced amacrine cells, which are already located in the RGC layer by 72 hpf (this work, and Chow et al., 2015). Interestingly, a similar expression pattern was described for the mouse retina (Erskine et al., 2000). On one hand, this supports the idea that the polarization of the signal is of importance and, on the other, it also suggests that *slit2* expression is not determined by cell identity but by cell position. Previous work in *Xenopus*, showing lower resolution images, have also indicated an early localization of *slit2* mRNA at the CMZ and, later, in the inner portion of the inner nuclear layer (Piper et al., 2006; Hocking et al., 2010). Nevertheless, we cannot ascertain if the observed thickening of the inner plexiform layer is related to an effect on RGCs. The *atoh7* null mutant zebrafish line *lakritz* completely lacks RGCs, and an inner plexiform layer with presynaptic sublaminae formed by bipolar cells, albeit delayed, still forms (Kay et al., 2004). Studies in which all four cell types contributing to this layer (RGCs, amacrine cells, bipolar cells and Müller glia) were genetically removed, individually or in combination, have indicated that each of them is sufficient to generate an inner plexiform layer-like structure (Randlett et al., 2013).

All the defects we observed related to RGCs axons were at their proximal extra-retinal portion. Our results indicated that maternally- and zygotically-expressed Slit2 is necessary for the correct fasciculation of these axons inside the optic nerve. This correlates well with previous reports that Slit2 promotes tighter fasciculation of RGC axons *in vitro* (Ringstedt et al., 2000). There are two main mechanisms that might

promote axon fasciculation at the optic nerve. One of them is cell adhesion, either between axons or with surrounding glial cells (see for example Masai et al., 2003; Bruce et al., 2017). The other one is given by repulsive interactions between axons and surrounding tissues (surround repulsion), which can also favor fasciculation by channeling axons into a common path, a mechanism that has been suggested for Slits (Rasband et al., 2003). Interestingly, we also observed apparent fasciculation defects in the axon tracts that form the anterior commissure (AC). Previous studies have found *slit2* expression in the region adjacent to the AC, as well as defects in axon guidance/organization of this commissure upon slit2 knock-down using morpholinos (Barresi et al., 2005; Hofmeister et al., 2012).

Functions in fasciculation have previously been attributed to the Slit-Robo signaling pathway in *Drosophila* (Bhat, 2017) and to Slit2 acting through Robo1 and Robo2 in mice (Jaworski and Tessier-Lavigne, 2012). The observed expression of *slit2* in cells closely surrounding the optic nerves from early stages strongly supports the idea that a channeling mechanism could be in place, delineating the path for RGC axons at the zebrafish optic nerve. Nevertheless, it should be considered that Slit-Robo signaling can also regulate cadherin-mediated cell adhesion in several systems, attenuating in some (Rhee et al., 2002; Santiago-Martínez et al., 2008) and potentiating in others (Shiau and Bronner-Fraser, 2009). As an example, Slit1b acting on nascent RGCs has a role in apical detachment through the regulation of N-cadherin in zebrafish embryos (Wong et al., 2012). Hence, an indirect effect of Slit2, modulating adhesion molecules such as N-cadherin, cannot be ruled out at this point.

In addition to the apparent defasciculation at the optic nerve, an important proportion of mutant embryos presented a very distinctive defect at the optic chiasm, where one of the optic nerves appeared split in two branches that surrounded the contralateral nerve. We found that the selection of which optic nerve splits, left or right, appears to be random. A role for Slit2 in optic chiasm formation has been previously shown in mice. Plump et al. found defects in *slit1-/-;slit2-/-* double mutants (Plump et al., 2002), but no detectable phenotype in *slit2-/-* mice. However, using a different quantification approach, Down et al. reported a defect of the *slit2-/-* chiasm, where many axons mislocated abnormally anteriorly (Down et al., 2013). It is possible that the missorting

we observed at the zebrafish optic chiasm comes as a result of axons misprojecting anteriorly, as was reported for mice optic fibers. However, higher temporal resolution is needed to answer this question and dissect the dynamics of axon sorting at the chiasm. A different scenario, i.e. that the phenotype reported here is not related to anteriorly projecting axons, cannot be disregarded. Discordant results in zebrafish and mouse would not be surprising given the intrinsic differences in optic chiasm organization between species. Mice possess some degree of binocular vision, which means that, although most RGC axons cross contralaterally, some take an ipsilateral turn at the optic chiasm (Jeffery and Erskine, 2005). Zebrafish, on the other hand, lack binocular vision and, hence, present only contralateral axon crossing. We and others (Hutson and Chien, 2002; Chalasani et al., 2007) found expression of *slit2* mRNA in cells located just anterior to the optic chiasm, which could be responsible for generating a gradient channeling the axons in this area. In addition, and this presents as another difference between the species, other Slits are co-expressed in these regions: Slit1 in mice and Slit3 in zebrafish (Rasband et al., 2003).

Interestingly, this "optic nerve splitting" effect was evident even in the heterozygous mutants, indicating allelic codominance, and it did not appear to be compensated by maternally-expressed mRNA. It is somehow unexpected that the frequency of errors is lower in *slit2*-/-^{mz} than in *slit2*-/- embryos. In principle, this could be due to the fact that the maternal zygotic mutants were obtained after more crossings than the zygotic mutants, hence favoring the accumulation of gene compensation effects (El-Brolosy and Stainier, 2017). Conversely, the axon fasciculation phenotype in the optic nerve was apparently maternally-compensated, as it was only evident in maternal homozygous mutants (*slit2*-/-^{mz}). These differences point to a higher sensitivity to Slit2 dosage, as well as a tighter time-dependent regulation, of axon crossing at the optic chiasm. As it has been suggested by previous research, the decision to cross the midline is probably one of the most delicately regulated steps in RGC axon growth to their targets (Rasband et al., 2003; Herrera et al., 2019).

Beyond the optic chiasm, RGC axons still have to travel a distance through the optic tracts to eventually arrive at the optic tectum, where they must properly sort to innervate certain areas according to a retinotopic map (Kita et al., 2015). We analyzed

these last steps in axon guidance/fasciculation and targeting by labeling RGC axons coming from different areas of the neural retina with lipophilic dyes. We found no defects in tract organization in morphant or mutant larvae, which also showed apparently normal naso-temporal and dorso-ventral retinotectal maps. Therefore, while *slit2* expression close to the proximal portion of optic tract opens the possibility for a role similar to the one observed in the optic nerves, this seems not to be the case. On the other hand, because we and others (Campbell et al., 2007) found no *slit2* expression at the optic tectum, the lack of a phenotype in this area comes as less surprising.

Altogether, our results show that *slit2* mutation caused a relatively "mild" phenotype when compared to that in other axon guidance molecule mutants. Although some evidence of the possibility of a small degree of genetic compensation was found, the similarity between the mutant and morphant phenotypes indicates that this was not a major factor. Our observations reinforce the idea that there is not one, but several, signaling molecules normally acting at the same time along the different steps in RGC axon extension, in accordance with the rich signaling molecule expression landscape that has been described in the retina and optic tectum, and all along the visual pathway (Herrera et al., 2019). In the zebrafish, these include other Slit factors such as Slit1a or Slit3, which could also act on Robo2 receptor, partly explaining the apparent discrepancy with the stronger phenotype in *astray*/Robo2 mutants at the optic chiasm, and optic tract (Fricke et al., 2001; Hutson and Chien, 2002). Nevertheless, we provide here conclusive evidence for an essential function of Slit2 in the organization of the proximal portion of the visual pathway of the zebrafish, comprising the optic nerve and optic chiasm.

REFERENCES

Almeida AD, Boije H, Chow RW, He J, Tham J, Suzuki SC, Harris WA. 2014. Spectrum of Fates: a new approach to the study of the developing zebrafish retina. Development 141:1971–1980.

Baier H, Klostermann S, Trowe T, Karlstrom RO, Nüsslein-Volhard C, Bonhoeffer F.

1996. Genetic dissection of the retinotectal projection. Development 123:415–425.

Barresi MJF, Hutson LD, Chien C-B, Karlstrom RO. 2005. Hedgehog regulated Slit expression determines commissure and glial cell position in the zebrafish forebrain. Development 132:3643–3656.

Bhat KM. 2017. Post-guidance signaling by extracellular matrix-associated Slit/Slit-N maintains fasciculation and position of axon tracts in the nerve cord. PLoS Genet 13:1–26.

Blockus H, Chédotal A. 2016. Slit-robo signaling. Dev 143:3037–3044.

Brose K, Tessier-Lavigne M. 2000. Slit proteins: Key regulators of axon guidance, axonal branching, and cell migration. Curr Opin Neurobiol 10:95–102.

Bruce FM, Brown S, Smith JN, Fuerst PG, Erskine L. 2017. DSCAM promotes axon fasciculation and growth in the developing optic pathway. Proc Natl Acad Sci U S A 114:1702–1707.

Campbell DS, Stringham SA, Timm A, Xiao T, Law M-Y, Baier H, Nonet ML, Chien C-B. 2007. Slit1a Inhibits Retinal Ganglion Cell Arborization and Synaptogenesis via Robo2-Dependent and -Independent Pathways. Neuron 55:231–245.

Chalasani SH, Sabol A, Xu H, Gyda MA, Rasband K, Granato M, Chien C-B, Raper JA. 2007. Stromal cell-derived factor-1 antagonizes slit/robo signaling in vivo. J Neurosci 27:973–980.

Choi J-H, Law M-Y, Chien C-B, Link BA, Wong RO. 2010. In vivo development of dendritic orientation in wild-type and mislocalized retinal ganglion cells. Neural Dev 5:29.

Chow RW, Almeida AD, Randlett O, Norden C, Harris WA. 2015. Inhibitory neuron migration and IPL formation in the developing zebrafish retina. Development 142:2665–2677.

Delloye-Bourgeois C, Jacquier A, Charoy C, Reynaud F, Nawabi H, Thoinet K, Kindbeiter K, Yoshida Y, Zagar Y, Kong Y, Jones YE, Falk J, et al. 2015. PlexinA1 is a new Slit

receptor and mediates axon guidance function of Slit C-terminal fragments. Nat Neurosci 18:36–45.

Down M, Willshaw DA, Pratt T, Price DJ. 2013. Steerable-filter based quantification of axonal populations at the developing optic chiasm reveal significant defects in Slit2-/- as well as Slit1-/-Slit2-/- embryos. BMC Neurosci 14:9.

El-Brolosy MA, Stainier DYR. 2017. Genetic compensation: A phenomenon in search of mechanisms. PLoS Genet 13:1–17.

Erskine L, Williams SE, Brose K, Kidd T, Rachel RA, Goodman CS, Tessier-Lavigne M, Mason CA. 2000. Retinal Ganglion Cell Axon Guidance in the Mouse Optic Chiasm: Expression and Function of Robos and Slits. J Neurosci 20:4975–4982.

Fricke C, Lee JS, Geiger-Rudolph S, Bonhoeffer F, Chien C-B. 2001. Astray, a Zebrafish Roundabout Homolog Required for Retinal Axon Guidance. Science 292:507–510.

Gibson DA, Tymanskyj S, Yuan RC, Leung HC, Lefebvre JL, Sanes JR, Chédotal A, Ma L. 2014. Dendrite self-avoidance requires cell-autonomous slit/robo signaling in cerebellar purkinje cells. Neuron 81:1040–1056.

Herrera E, Erskine L, Morenilla-Palao C. 2019. Guidance of retinal axons in mammals. Semin Cell Dev Biol 85:48–59.

Hocking JC, Hehr CL, Bertolesi GE, Wu JY, McFarlane S. 2010. Distinct roles for Robo2 in the regulation of axon and dendrite growth by retinal ganglion cells. Mech Dev 127:36–48.

Hofmeister W, Devine CA, Rothnagel JA, Key B. 2012. Frizzled-3a and slit2 genetically interact to modulate midline axon crossing in the telencephalon. Mech Dev 129:109–124.

Howitt JA, Clout NJ, Hohenester E. 2004. Binding site for Robo receptors revealed by dissection of the leucine-rich region of Slit. EMBO J 23:4406–4412.

Hutson LD, Chien C-B. 2002. Pathfinding and error correction by retinal axons: The role of astray/robo2. Neuron 33:205–217.

Hutson LD, Jurynec MJ, Yeo SY, Okamoto H, Chien C-B. 2003. Two Divergent slit1 Genes in Zebrafish. Dev Dyn 228:358–369.

Jao L-E, Wente SR, Chen W. 2013. Efficient multiplex biallelic zebrafish genome editing using a CRISPR nuclease system. Proc Natl Acad Sci U S A 110:13904–13909.

Jaworski A, Tessier-Lavigne M. 2012. Autocrine/juxtaparacrine regulation of axon fasciculation by Slit-Robo signaling. Nat Neurosci 15:367–369.

Jeffery G, Erskine L. 2005. Variations in the architecture and development of the vertebrate optic chiasm. Prog Retin Eye Res 24:721–753.

Kay JN, Roeser T, Mumm JS, Godinho L, Mrejeru A, Wong ROL, Baier H. 2004. Transient requirement for ganglion cells during assembly of retinal synaptic layers. Development 131:1331–1342.

Kimmel CB, Ballard WW, Kimmel SR, Ullmann B, Schilling TF. 1995. Stages of embryonic development of the zebrafish. Dev Dyn 203:253–310.

Kita EM, Scott EK, Goodhill GJ. 2015. Topographic wiring of the retinotectal connection in zebrafish. Dev Neurobiol 75:542–556.

Koziol U, Rauschendorfer T, Zanon Rodríguez L, Krohne G, Brehm K. 2014. The unique stem cell system of the immortal larva of the human parasite Echinococcus multilocularis. Evodevo 5:10.

Lee J, Ray R, Chien C-B. 2001. Cloning and Expression of Three Zebrafish Roundabout Homologs Suggest Roles in Axon Guidance and Cell Migration. 230:216–230.

Lepanto P, Davison C, Casanova G, Badano JL, Zolessi FR. 2016. Characterization of primary cilia during the differentiation of retinal ganglion cells in the zebrafish. Neural Dev 11:10.

Macdonald R, Scholes J, Strähle U, Brennan C, Holder N, Brand M, Wilson SW. 1997. The Pax protein Noi is required for commissural axon pathway formation in the rostral forebrain. Development 124:2397–2408.

Masai I, Lele Z, Yamaguchi M, Komori A, Nakata A, Nishiwaki Y, Wada H, Tanaka H,

Nojima Y, Hammerschmidt M, Wilson SW, Okamoto H. 2003. N-cadherin mediates retinal lamination, maintenance of forebrain compartments and patterning of retinal neurites. Development 130:2479–2494.

Moreno-Mateos MA, Vejnar CE, Beaudoin J, Fernandez JP, Mis EK, Khokha MK, Giraldez AJ. 2015. CRISPRscan: designing highly efficient sgRNAs for CRISPR-Cas9 targeting in vivo. Nat Methods 12:982–988.

Nguyen Ba-Charvet KT, Brose K, Ma L, Wang KH, Marillat V, Sotelo C, Tessier-Lavigne M, Chédotal A. 2001. Diversity and specificity of actions of Slit2 proteolytic fragments in axon guidance. J Neurosci 21:4281–4289.

Niclou SP, Jia L, Raper JA. 2000. Slit2 is a repellent for retinal ganglion cell axons. J Neurosci 20:4962–4974.

Park KW, Morrison CM, Sorensen LK, Jones CA, Rao Y, Chien C-B, Wu JY, Urness LD, Li DY. 2003. Robo4 is a vascular-specific receptor that inhibits endothelial migration. Dev Biol 261:251–267.

Piper M, Anderson R, Dwivedy A, Weinl C, Horck F Van, Leung KM, Cogill E, Holt C. 2006. Signaling mechanisms underlying Slit2-induced collapse of Xenopus retinal growth cones. Neuron 49:215–228.

Plump AS, Erskine L, Sabatier C, Brose K, Epstein CJ, Goodman CS, Mason CA, Tessier-Lavigne M. 2002. Slit1 and Slit2 cooperate to prevent premature midline crossing of retinal axons in the mouse visual system. Neuron 33:219–232.

Prieto D, Aparicio G, Morande PE, Zolessi FR. 2014. A fast, low cost, and highly efficient fluorescent DNA labeling method using methyl green. Histochem Cell Biol 142:335–345.

Randlett O, MacDonald RB, Yoshimatsu T, Almeida AD, Suzuki SC, Wong RO, Harris WA. 2013. Cellular Requirements for Building a Retinal Neuropil. Cell Rep 3:282–290.

Rasband K, Hardy M, Chien C-B. 2003. Generating X: Formation of the optic chiasm. Neuron 39:885–888.

Rhee J, Mahfooz NS, Arregui C, Lilien J, Balsamo J, VanBerkum MFA. 2002. Activation of the repulsive receptor roundabout inhibits N-cadherin-mediated cell adhesion. Nat Cell Biol 4:798–805.

Ringstedt T, Braisted JE, Brose K, Kidd T, Goodman C, Tessier-Lavigne M, O'Leary DDM. 2000. Slit inhibition of retinal axon growth and its role in retinal axon pathfinding and innervation patterns in the diencephalon. J Neurosci 20:4983–4991.

Santiago-Martínez E, Soplop NH, Patel R, Kramer SG. 2008. Repulsion by Slit and Roundabout prevents Shotgun/E-cadherin-mediated cell adhesion during Drosophila heart tube lumen formation. J Cell Biol 182:241–248.

Schindelin J, Arganda-Carreras I, Frise E, Kaynig V, Longair M, Pietzsch T, Preibisch S, Rueden C, Saalfeld S, Schmid B, Tinevez J-Y, White DJ, et al. 2012. Fiji: an open-source platform for biological-image analysis. Nat Methods 9:676–682.

Seiradake E, Philipsborn AC von, Henry M, Fritz M, Lortat-Jacob H, Jamin M, Hemrika W, Bastmeyer M, Cusack S, McCarthy AA. 2009. Structure and functional relevance of the Slit2 homodimerization domain. EMBO Rep 10:736–741.

Shiau CE, Bronner-Fraser M. 2009. N-cadherin acts in concert with Slit1-Robo2 signaling in regulating aggregation of placode-derived cranial sensory neurons. Development 136:4155–4164.

Steigemann P, Molitor A, Fellert S, Jäckle H, Vorbrüggen G. 2004. Heparan Sulfate Proteoglycan Syndecan Promotes Axonal and Myotube Guidance by Slit/Robo Signaling. Curr Biol 14:225–230.

Thompson H, Andrews W, Parnavelas JG, Erskine L. 2009. Robo2 is required for Slit-mediated intraretinal axon guidance. Dev Biol 335:418–426.

Thompson H, Camand O, Barker D, Erskine L. 2006. Slit proteins regulate distinct aspects of retinal ganglion cell axon guidance within dorsal and ventral retina. J Neurosci 26:8082–8091.

Wang KH, Brose K, Arnott D, Kidd T, Goodman CS, Henzel W, Tessier-Lavigne M. 1999. Biochemical purification of a mammalian slit protein as a positive regulator of sensory

axon elongation and branching. Cell 96:771–784.

Whitford KL, Marillat V, Stein E, Goodman CS, Tessier-Lavigne M, Chédotal A, Ghosh A. 2002. Regulation of cortical dendrite development by Slit-Robo interactions. Neuron 33:47–61.

Wong GKW, Baudet M-L, Norden C, Leung L, Harris WA. 2012. Slit1b-Robo3 signaling and N-cadherin regulate apical process retraction in developing retinal ganglion cells. J Neurosci 32:223–228.

Wright KM, Lyon KA, Leung H, Leahy DJ, Ma L, Ginty DD. 2012. Dystroglycan Organizes Axon Guidance Cue Localization and Axonal Pathfinding. Neuron 76:931–944.

Xiao T, Staub W, Robles E, Gosse NJ, Cole GJ, Baier H. 2011. Assembly of lamina-specific neuronal connections by slit bound to type IV collagen. Cell 146:164–176.

Yeo SY, Little MH, Yamada T, Miyashita T, Halloran MC, Kuwada JY, Huh TL, Okamoto H. 2001. Overexpression of a slit homologue impairs convergent extension of the mesoderm and causes cyclopia in embryonic zebrafish. Dev Biol 230:1–17.

Zolessi FR, Poggi L, Wilkinson CJ, Chien C-B, Harris WA. 2006. Polarization and orientation of retinal ganglion cells in vivo. Neural Dev 1:2.

FIGURE LEGENDS

Figure 1. Expression of *slit2* in the developing neural retina. Expression of *slit2* in the zebrafish retina, evidenced through fluorescent *in situ* hybridization (FISH) and confocal imaging. **(a,b)** Two different single confocal planes of a 40 hpf wild-type embryo. *slit2* signal can be observed in the ciliary margin zone (brackets in a) and in cells located at the amacrine cell region in the central retina (arrowheads in b). See Supplementary Video 1. **(c,d)** Single confocal planes of 48 hpf wild-type embryos, at different magnifications. *slit2* expression is evident in putative amacrine cell bodies (arrowheads) and in the forming inner plexiform layer (arrows). See Supplementary Video 2. **(e)**

Control FISH (sense probe) on a 48 hpf embryo. **(f,g)** Single confocal planes of 72 hpf wild-type embryos. s*lit2* expression in putative amacrine cells becomes more evident by this stage (represented in the diagram in g'). See Supplementary Video 3. **(h)** Single confocal plane of 72 hpf SoFa1 embryos injected with control or *ptf1a* morpholinos (MO). RGCs are labeled by *atoh7*:Gap43-mRFP expression, while amacrine and horizontal cells express *ptf1a*:EGFP. In morphant embryos, amacrine cells disappear and the IPL is reduced and loses its synaptic sublaminae (arrows). **(i)** Maximum intensity z-projection of a 72 hpf wild-type embryo injected with *ptf1a* MO1+MO2, and labeled by *in situ* hybridization to *slit2*. Most of the s*lit2* expression at the inner nuclear layer disappears. CMZ: ciliary margin zone; GCL: ganglion cells layer; INL: inner nuclear layer; IPL: inner plexiform layer; L: lens; NR: neural retina; ONL: outer nuclear layer; OPL: outer plexiform layer. Scale bars: a, b, c, e, f: 40 µm; d: 15 µm; g: 20 µm; h: 10 µm; i: 40 µm.

Figure 2. Expression of *slit2* along the pathway of RGC axons. Expression of *slit2* in the zebrafish brain, evidenced through fluorescent *in situ* hybridization and confocal imaging. **(a)** Maximum intensity z-projection of the cephalic region of a 40 hpf wild-type embryo (ventral view). In addition to the signal on putative amacrine cells in the retina described in Fig. 1 (arrowhead), *slit2* expression is evident around the intra- and extra-retinal optic nerve (ION and EON, respectively). This can be clearly visualized in the magnified orthogonal section a'. *slit2* is also expressed in two bilateral cell clusters in the ventro-rostral diencephalon (arrows). See Supplementary Video 4. **(b,c)** Two different confocal planes of a 48 hpf wild-type embryo. *slit2*expression is evident in cells surrounding the optic nerves (ON) and anterior to the optic tracts and optic chiasm (OT and OC, respectively). This can be clearly visualized in the orthogonal sections b' and b'', and in the higher magnification image in c'. See Supplementary Video 5. **(d,e)** Maximum intensity z-projection and single confocal plane, respectively, of 72 hpf wild-type embryos. Although a strong signal is clearly visible in amacrine cells, no expression of *slit2* is observed around the optic chiasm (d) or the optic tectum (dotted line; e) at this stage. However, a heterogeneously distributed signal can be observed in the forebrain (FB). NP: nasal pit; NR: neural retina. Scale bars: a-e, b' and b'': 40 µm; a', a'': 20 µm; c': 15 µm.

Figure 3. The NM_131753.1:g.30_39del mutant line presents a 10 base pair deletion in the first exon of the *slit2* gene. (a) Initial coding sequence of the wild-type and CRISPR-Cas9-mutated *slit2* gene. The initiation ATG codon is marked in bold and the sgRNA target sequence is underlined. A 10 base-pair deletion can be observed in the mutated sequence. **(b)** N-terminal sequence of the Slit2 protein. The deletion results in an mRNA coding sequence frameshift, causing a change in the protein sequence from amino acid L12 (arrow) onwards and the subsequent introduction of a premature STOP codon. **(c)** Diagram showing the different Slit2 protein domains. The termination of translation due to the premature STOP codon occurs at the region encoding the signal peptide (scissors), resulting in a protein truncated before the first LRR domain. **(d)** Low magnification images of 48 hpf embryos show no evident external defects in *slit2* mutants from either heterozygous (*slit2-/-*) or homozygous (*slit2-/-^{mz}*) parents. Some embryos injected with *slit2* MO exhibited mild defects such as cardiac (arrowhead) or cephalic (arrow) oedema. Scale bar: 500 µm.

Figure 4. Effect of *slit2* mutation on the retinal inner plexiform layer. (a) Single confocal planes from cryosections of 5 dpf larvae, labeled with phalloidin-rhodamine and methyl green. Neither the retina laminar organization, nor the inner plexiform layer sub-lamination, are visibly affected in mutant larvae. **(b-d)** Measurements of ganglion cell layer, inner plexiform layer and whole retina thickness. There are no significant differences for the absolute values between wild-type and mutant situations (b), and in both wild-type and *slit2-/-^{mz}* larvae, there is a linear correlation between the thickness of ganglion cell layer and inner plexiform layer and the thickness of the retina (c). The proportional thickness of the ganglion cell layer, GCL/retina shown in (d), does not vary in mutants. However, the inner plexiform layer appears slightly but significantly thicker in relation to the whole retina in both *slit2-/-* and *slit2-/-^{mz}* larvae (d, IPL/retina). n larvae (n experiments) = 40 (4) *slit2+/+*, 18 (2) *slit2+/-*, 20 (2) *slit2-/-* and 46 (3) *slit2-/-^{mz}*; (b) and (d) show mean +/- SD; Student's *t* test. GCL: ganglion cell layer; INL: inner nuclear layer; IPL: inner plexiform layer; ONL: outer nuclear layer; OPL: outer plexiform layer. Scale bar: 10 µm.

Figure 5. Effects of *slit2* mutation on optic nerve morphology. (a,b) Maximum intensity z-projections of 48 hpf embryos immunostained to label RGCs (zn8 antibody). In *slit2-/-*

mutant embryos, defects can be observed in nerve crossing at the optic chiasm (arrowhead; see Supplementary Video 6). In *slit2-/-^{mz}* embryos optic nerves appear thickened (arrows), which is better shown in the magnified single confocal planes in b' and b''. **(c)** Diagram showing the measured structures displayed in the graphs in e. **(d)** Fluorescence intensity profile of zn8 signal in the optic nerves, measured along the yellow transects in b' and b''. In addition to being wider, the *slit2-/-^{mz}* profile shows identifiable spikes indicating axon defasciculation. **(e)** Measurement of the optic nerve diameter compared to the retina thickness. While the intra-retinal portion (left) showed no variation, the extra-retinal optic nerve (right) was significantly thicker in *slit2-/-^{mz}* embryos. n nerves/embryos (n experiments) = 18 (3) *slit2+/+*, 28 (3) *slit2+/-*, 25 (3) *slit2-/-*, 41 (3) *slit2-/-^{mz}*, 31 (3) control MO, 38 (3) *slit2* MO; mean +/- SD; Student's *t* test. EON: extra-retinal optic nerve; ION: intra-retinal optic nerve; NR: neural retina. Scale bars: a, b: 50 µm; b', b'': 25 µm.

Figure 6. Effects of *slit2* mutation on optic chiasm formation. RGC axons from both eyes were anterogradely labeled by DiI or DiO injection into the retina, to better characterize the defects at the optic chiasm. **(a,b)** Horizontal maximum intensity z-projections of 48 hpf embryos, at the level of the optic chiasm, with magnified orthogonal sections at the sagittal plane level (dotted line). The DiI/DiO separated channels show thick maximum intensity projections, including the proximal portion of the optic tracts, while in the merged images, the stacks only include the optic nerve and chiasm. In the wild-type embryos, axons from one nerve cross caudal and slightly dorsal to those from the contralateral nerve. In *slit2* mutant (a) and morphant (b) embryos, however, one of the nerves is frequently split into two groups of axons (marked with arrowheads in the orthogonal sections). See Supplementary Videos7 and 8. **(c)** Diagram showing the strategy used for anterograde axon labeling. **(d)** Quantification of phenotype penetrance in mutant and morphant embryos. *slit2+/-*, *slit2-/-*, *slit2-/-^{mz}* and *slit2* morphant embryos all show a significant increase in optic nerve crossing defects when compared to their respective controls (wild type and control MO injection), albeit to different extents. n embryos (n independent experiments) = 33 (3) *slit2+/+*, 102 (3) *slit2+/-*, 50 (3) *slit2-/-*, 119 (3) *slit2-/-^{mz}*, 112 (3) control MO, 140 (3) *slit2* MO; mean +/- SD; Student's *t* test. **(e)** Relative frequency of left vs right optic nerve splitting in mutant

and morphant embryos, compared to the frequency of left vs right nerve crossing ventrally or dorsally in wild-type embryos (same embryos as in (d)). In all cases the values are very close to 50%. Scale bars: a, b: 40 µm; orthogonal sections: 20 µm.

Figure 7. *slit2* does not play a role in axon sorting at the optic tract or optic tectum. Retinotopic anterograde RGC axon labeling using DiI and DiO. **(a)** Parasagittal and frontal maximum intensity z-projections of the optic tract and tectal innervation of 5 dpf larvae revealed no differences in axon sorting between *slit2+/+* and *slit2-/-*^{mz}, after either nasal/temporal or dorsal/ventral DiO and DiI injection, respectively, as depicted in the drawings (a'). **(b)** Fluorescent intensity profiles through the optic tracts, following transects depicted as lines in a. **(c)** Horizontal maximum intensity z-projections of the optic tract and tectal innervation of 5 dpf larvae revealed no effects on the retinotectal maps, in mutant and morphant situations. Injection and resulting expected labeling are depicted in c'. Scale bars: a: 40 µm; c: 30 µm.

Supplementary material legends

Supplementary Figure 1. *slit2* expression at early developmental stages. Expression of *slit2* in the cephalic region of 24 and 30 hpf zebrafish embryos, evidenced through fluorescent *in situ* hybridization and confocal imaging. **(a)** Parasagittal maximum intensity z-projection of the anterior region (including forebrain, midbrain and hindbrain) of 24 and 30 hpf embryos. A strong signal was observed along the floor plate (FP) and, much fainter, on the mesencephalic roof (MR) only at 24 hpf. **(b)** Horizontal maximum intensity z-projection of the cephalic region (including forebrain, midbrain and eyes) of 24 and 30 hpf embryos, where *slit2* signal can be observed in different cell clusters, particularly at 30 hpf (the strong fluorescence on the ventricular surface is most probably non-specific). **(c)** Parasagittal single confocal section of the eye, showing no detectable expression in the retina at 24 or 30 hpf. **(d)** Confocal section from control embryos (sense probe). E: eye; FB: forebrain; FP: floor plate; FV: fourth ventricle; L: lens; MR: mesencephalic roof; NP: nasal pit; NR: neural retina; RL: rhombic lip. Scale bars: a: 80 µm; b: 30 µm; c, d: 40 µm.

Supplementary Figure 2. Expression of *slit2* in the retina is restricted to amacrine cells. Maximum intensity projections from 72 hpf embryos labeled by in situ hybridization to *slit2*, and injected with control or *ptf1a* morpholino oligomers. In morphant embryos, slit2 signal disappears selectively in amacrine cells of the retina (arrowheads), while it is maintained at the floorplate. FP: floor plate; L: lens; MR: mesencephalic roof; NR: neural retina. Scale bar: 60 µm.

Supplementary Figure 3. The NM_131753.1:g.30_39del mutant line can be identified by gel electrophoresis. Polyacrylamide gel electrophoresis of genomic PCR amplification products surrounding the sgRNA target sequence, from wild-type (WT), heterozygous mutant (HET) and homozygous mutant (MUT) individuals. The occurrence of the mutation can be readily identified, making it possible to differentiate the three genotypes. Heteroduplex formation in amplicons from heterozygous fish can be observed as characteristic lagging bands (asterisks).

Supplementary Figure 4. Absence of visible intraretinal axon guidance or RGC layer formation defects in *slit2* mutants or morphants. (a) Horizontal maximum intensity z-projections of the retina of 48 hpf embryos after immunolabeling RGCs with zn8 antibody. No RGC axons were seen growing inside the neural retina in neither morphant nor mutant embryos. The crossing defects at the optic chiasm were evident in some embryos (arrow). **(b)** Quantification of the retinal and ganglion cell layer volumes in 48 hpf *slit2+/+* and *slit2-/-*^{mz} embryos labeled as in (a). Although there is a mild apparent increase in total retinal volume in mutants, the statistical significance is very low (p=0.02), and no significant differences were determined for the ratio RGCs/Retina. n embryos (n experiments) = 15 (2) *slit2+/+*, 14 (2) *slit2-/-*^{mz}. Mean +/- SD. Student's *t* test. Scale bar: 40 µm.

Supplementary Figure 5. Slit2 is important for anterior commissure axon fasciculation and guidance. Immunolabeling of axons with anti-acetylated α-tubulin antibody on 30 and 40 hpf embryos. **(a)** Maximum intensity z-projection of the cephalic region of 30 hpf*slit2+/+*and *slit2-/-*^{mz} embryos (upper row: ventral view). Axons from the nuclei of the tract of the anterior and post-optic commissures (NTAC and NTPOC, respectively) can be seen crossing the midline, forming the anterior commissure (AC) and the post-optic

commissure (POC). This can be further visualized in the chosen frame from the 3D-projection shown in the middle row, where misguided axons can be seen along the AC in the mutant embryo (arrowheads). The axons that form the AC are tightly fasciculated in the wild-type and partially defasciculated in the mutant, as is visible in the magnified frontal view on the lower row. **(b)** Similar images to (a), from 40 hpf embryos. By this stage, more axons have incorporated into both the AC and the POC. The AC is notoriously wider in mutant than in wild-type embryos, as is clearly visible in the magnified frontal view on the lower row. **(c)**Fluorescent intensity profiles through the AC, following transects depicted as lines in the AC images on the lower row in (a) and (b). Scale bars: upper and middle row: 40 µm; lower row: 60µm.

Supplementary Figure 6. Slit2 is not essential for midline crossing of Mauthner cell axons. Immunolabeling of Mauthner cells with 3A10 antibody on 48 hpf embryos. No axon guidance defects are observed in these cells, in neither mutant nor morphant embryos. Scale bar: 30 µm.

Supplementary Video 1. *slit2* is expressed in the ciliary margin zone and putative amacrine cells at 40 hpf. 3D projection of a z-stack of a 40 hpf retina after fluorescent *in situ* hybridization for *slit2*. Signal can be observed at the ciliary margin zone, as well as in cells positioned in the middle region of the retina, which will probably give rise to amacrine cells. Corresponding to Fig. 1a,b.

Supplementary Video 2. *slit2* is expressed by amacrine cells at 48 hpf. 3D projection of a z-stack of a 48 hpf retina after fluorescent *in situ* hybridization for *slit2*. By this stage, signal can no longer be detected at the ciliary margin zone, while the expression by amacrine cells becomes stronger. Corresponding to Fig. 1c.

Supplementary Video 3. *slit2* is expressed by amacrine cells at 72 hpf. 3D projection of z-stack of a 72 hpf retina after fluorescent *in situ* hybridization for *slit2*. By this stage, amacrine cells are the only expressing cells in the retina. Corresponding to Fig. 1f.

Supplementary Video 4. *slit2* is expressed at the optic nerve exit at 40 hpf.3D projection of a z-stack of the cephalic region of a 40 hpf embryo after fluorescent *in situ*

hybridization for *slit2*. Signal can be detected at the optic nerve exit, as well as in two bilateral structures located in the forebrain. Corresponding to Fig. 2a.

Supplementary Video 5. *slit2* is expressed in cells surrounding the optic nerve at 48 hpf. 3D projection a z-stack of the cephalic region of a 48 hpf embryo after fluorescent *in situ* hybridization for *slit2*. Signal can be detected in cells located around the optic nerves, as well as in a few cells just anterior to the optic chiasm and tract. Corresponding to Fig. 2b,c.

Supplementary Video 6. Slit2 is important for nerve crossing at the optic chiasm. Z-stacks showing the optic chiasm of *slit2+/+* and *slit2-/-* embryos at 48 hpf, after immunostaining with zn8 antibody. In *slit2+/+* embryos, one optic nerve can be seen crossing ventrally to the contralateral nerve, while in *slit2-/-* one of the optic nerves splits and surrounds the contralateral nerve. The stack sequence is shown from the ventral to the dorsal region of the embryo. See Fig. 4a.

Supplementary Video 7. In wild-type embryos one optic nerve crosses ventrally to the contralateral nerve at the optic chiasm. 3D projection of a z-stack of the optic chiasm of a wild-type embryo injected with control MO and observed at 48 hpf, where RGC axons from both eyes were labeled anterogradely with either DiI or DiO. One of the optic nerves can be seen crossing rostrally and slightly ventral to the contralateral nerve, while remaining physically separate. Corresponding to Fig. 5b.

Supplementary Video 8. Slit2 is important for nerve crossing at the optic chiasm. 3D projection of a z-stack of the optic chiasm of a *slit2* morphant embryo at 48 hpf, where RGC axons from both eyes were labeled anterogradely with either DiI or DiO. One of the optic nerves splits into two groups of axons which surround the contralateral nerve. Corresponding to Fig. 5b.

Fig. 1

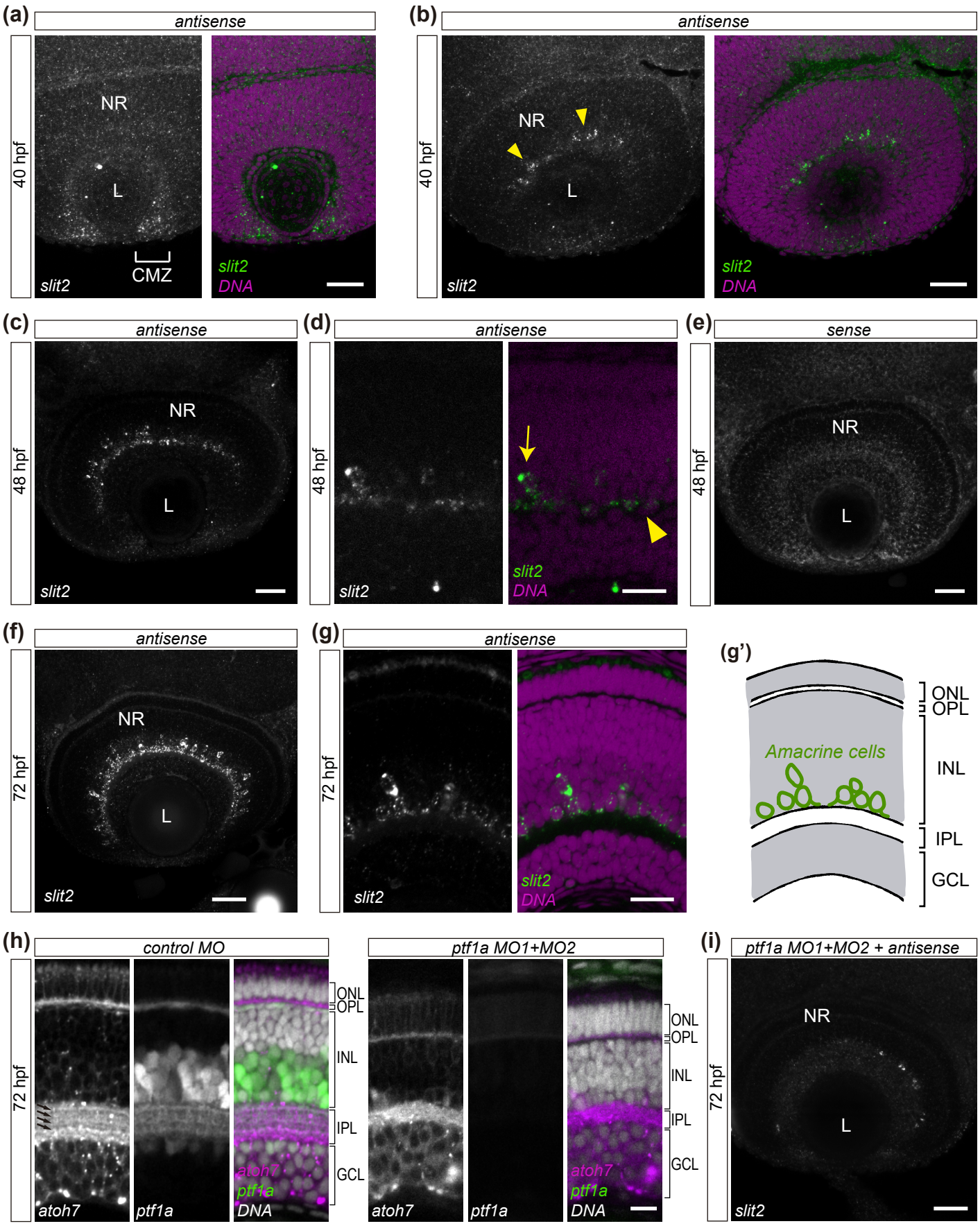

Fig. 2

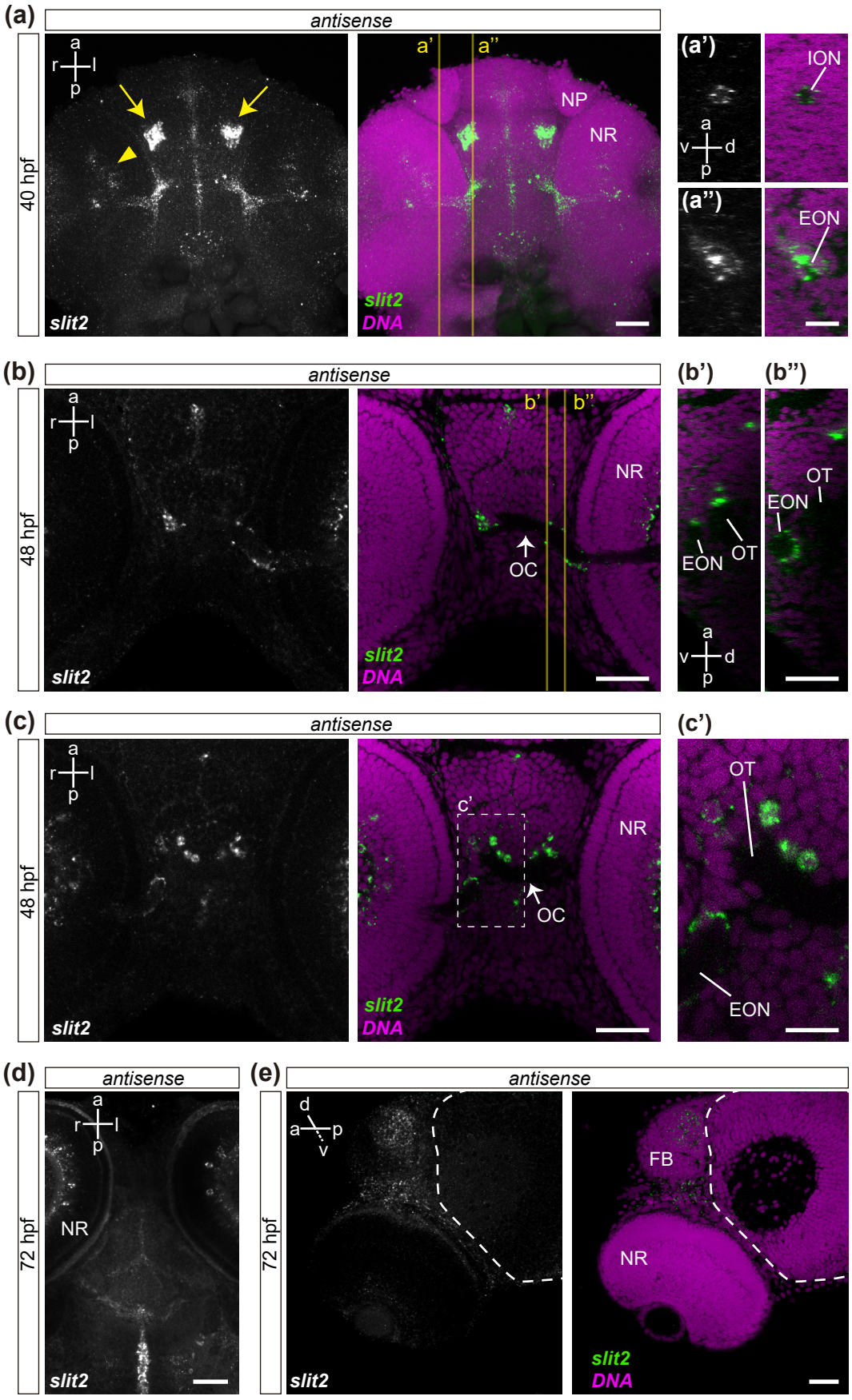

Fig. 3

(a)

slit2 gene

wild-type GCGGTG**ATG**TTTGTGTTGAAATCAGTGGTGCTCTGTGCGTTGCTCTGCGGGGC

mutant GCGGTG**ATG**TTTGTGTTGAAATCAGTGGTGCTCTG----------TGCGGGGC

(b)

Slit2 protein

wild-type **Met**FVLKSVVLCALLCGAGAQSCPSQCSCSGTAVDCHGQSLRSVPRNIPRNVERLDL

mutant **Met**FVLKSVVLCAGLEPSRARPSAPAAGQRWTATARVCGACRGTFPATLSDWT**Stop**

(c)

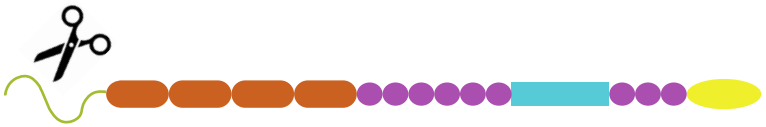

Signal peptide ***Laminin-G-like domain***

LRR domains (1-4) ***Cysteine knot***

EGF-like domains (1-6/7-9)

(d)

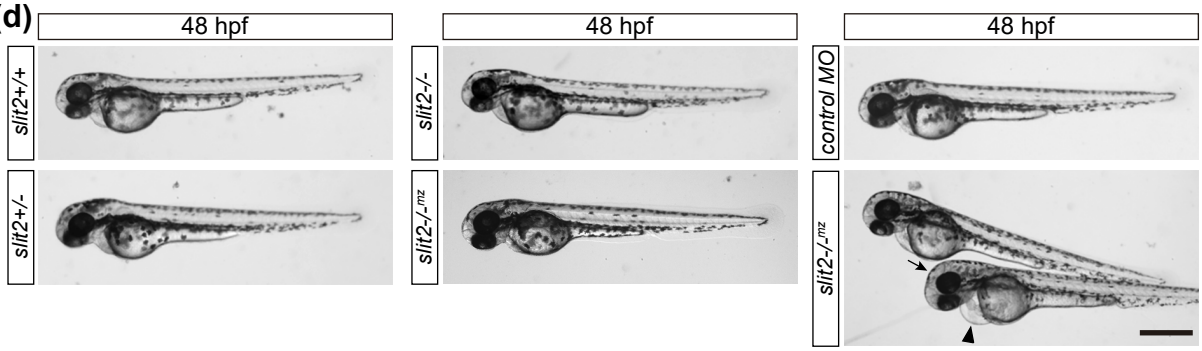

Fig. 4

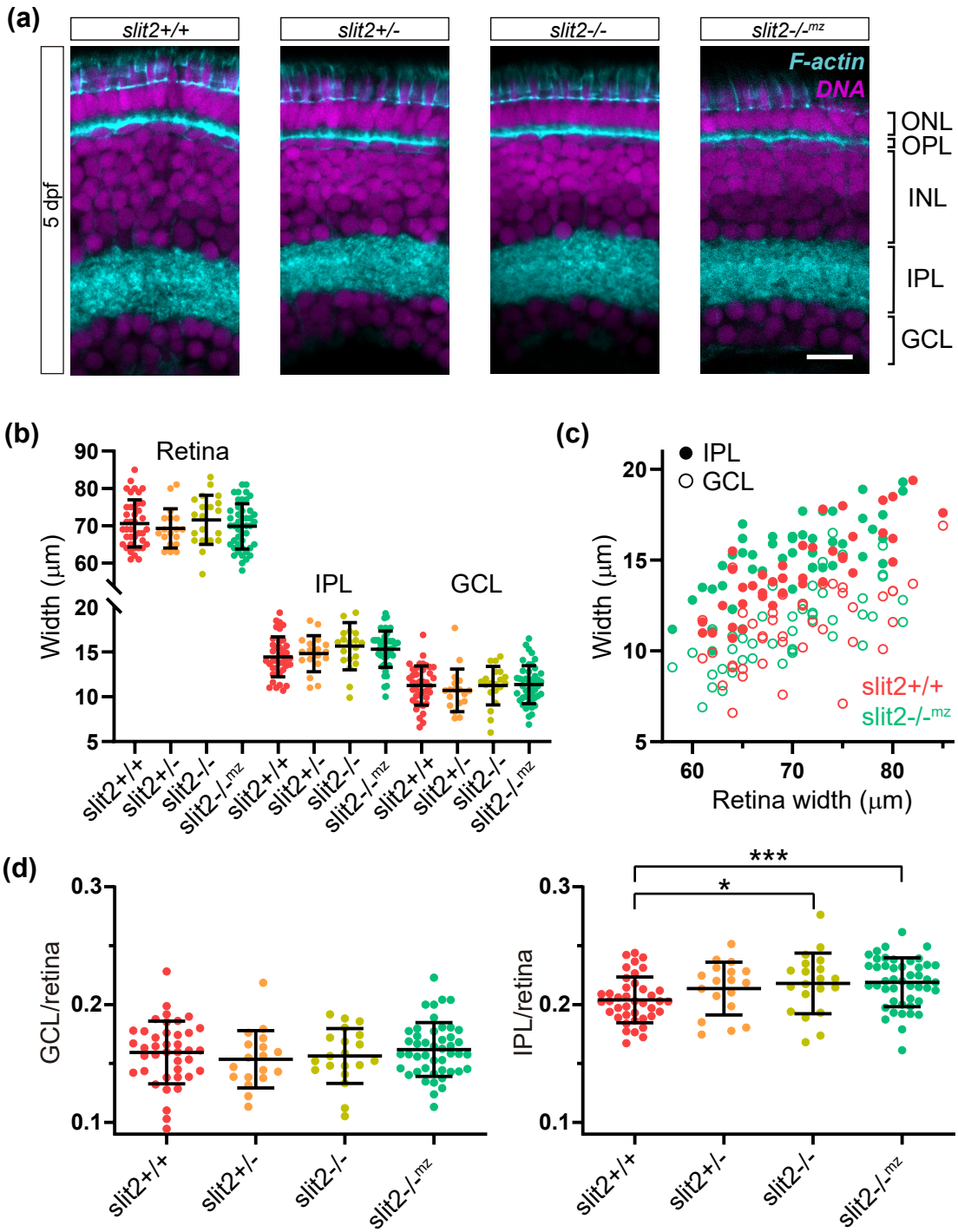

Fig. 5

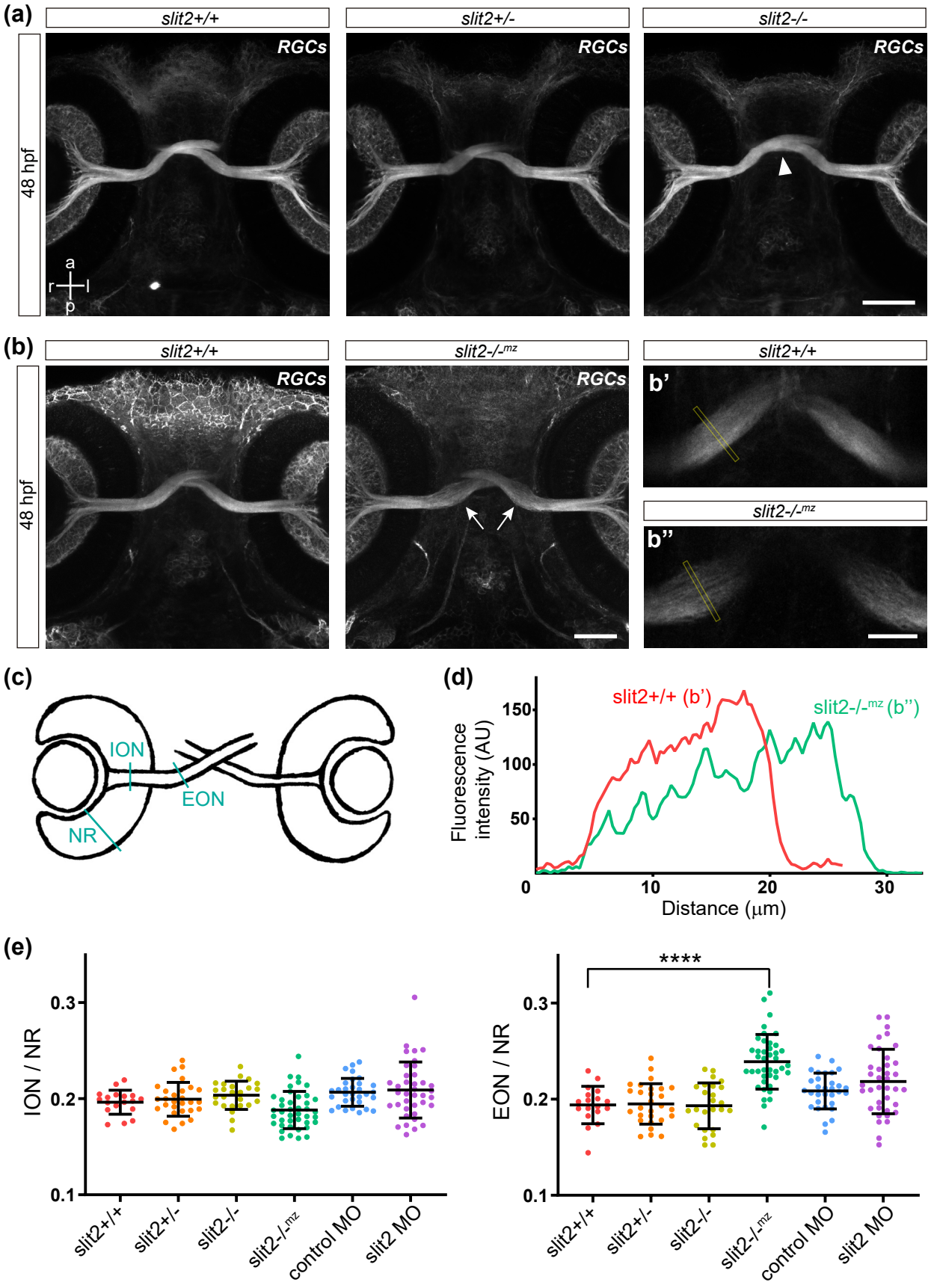

Fig. 6

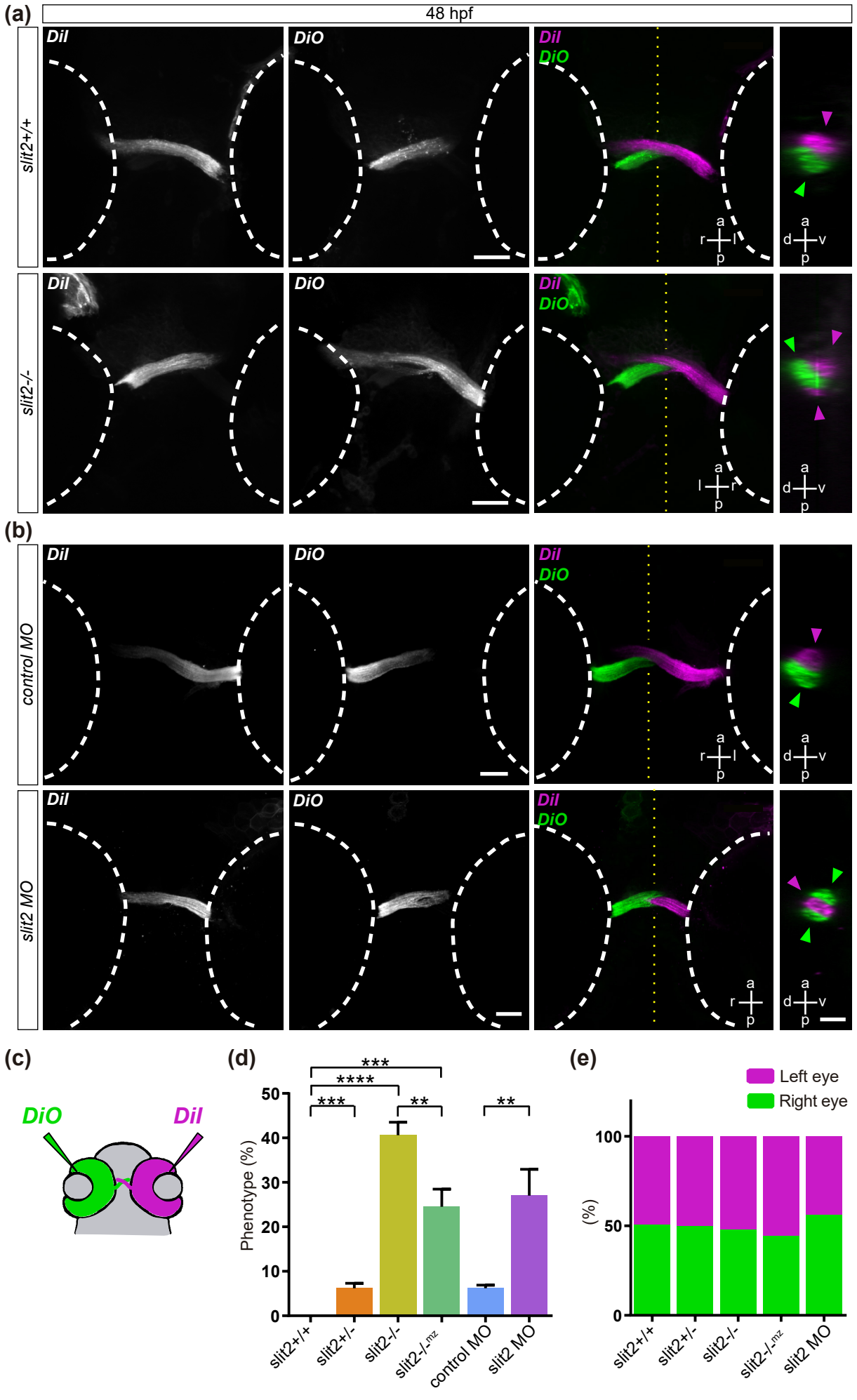

Fig. 7

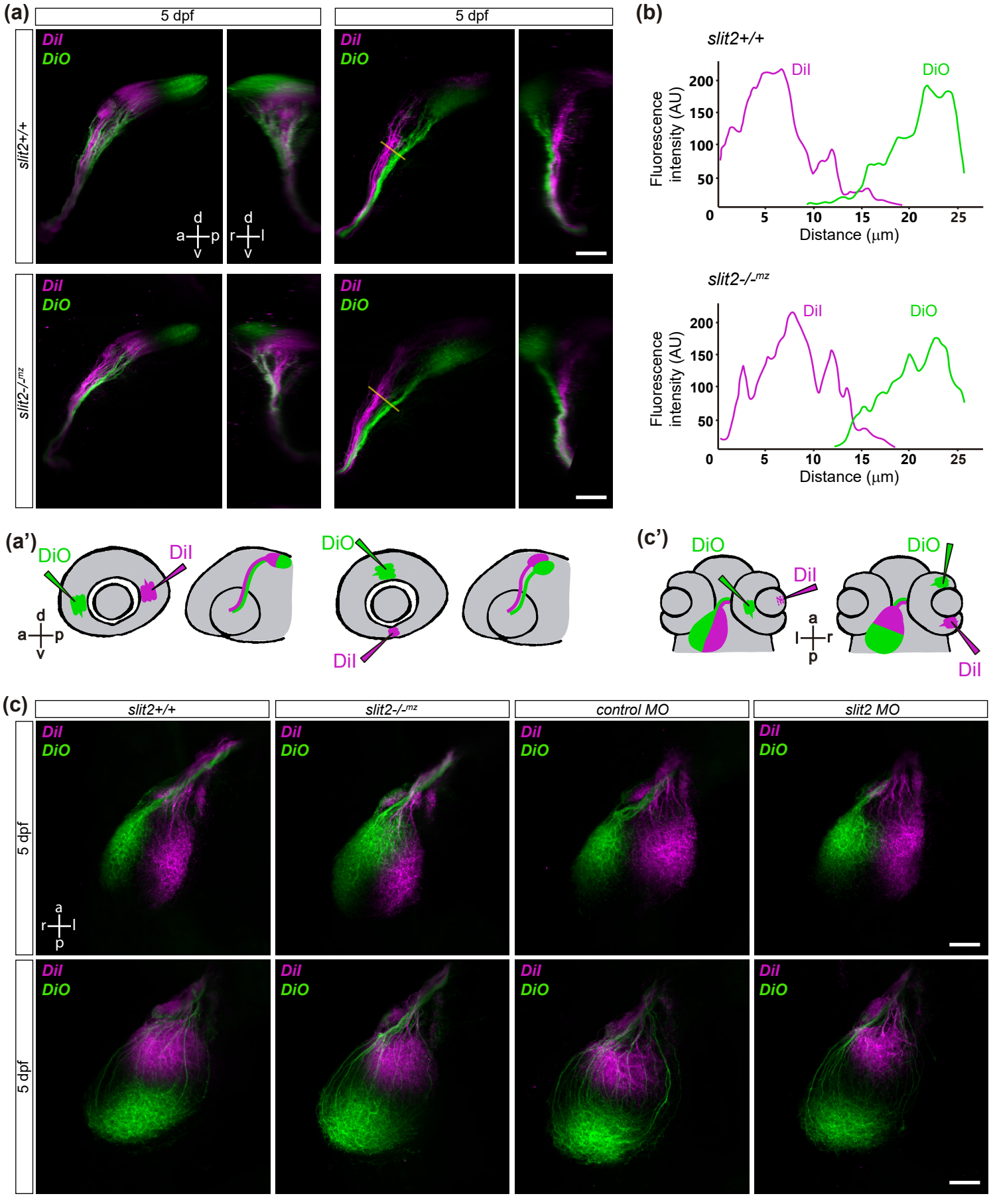

SUPPLEMENTARY TABLES

Table 1.

slit2 probe - forward primer	TAATACGACTCACTATAGGCAACAGAGAATCCTTCCTGC
slit2 probe - reverse primer	ATTTAGGTGACACTATAGATGCGTCTGATAGTGATCTCG
standard control morpholino	CCTCTTACCTCAGTTACAATTTATA
slit2 morpholino	CATCACCGCTGTTTCCTCAAGTTCT
ptf1a morpholino 1	CCAACACAGTGTCCATTTTTTGTGC
ptf1a morpholino 2	TTGCCCAGTAACAACAATCGCCTAC
sgRNA *slit2* 21	TAATACGACTCACTATAGGGCTCTGTGCGTTGCTCTGGTTTTAGAGCTA GAA
sgRNA *slit2* 71	TAATACGACTCACTATAGGGCTCCTGCAGCGGGACAGGTTTTAGAGCT AGAA
sgRNA *slit2* 700	TAATACGACTCACTATAGGCGATGTTGTGGCCCCTAAGTTTTAGAGCTA GAA
sgRNA *slit2* 819	TAATACGACTCACTATAGGAGTGGACTGCCGGGGGAAGTTTTAGAGCT AGAA

Table 2.

slit2 wild-type	**ATG**TTTGTGTTGAAATCAGTGGTGCTCTGTGCG TTGCTCTGCGGGGCTGGAGCCCAGTCGTG	
slit2 mutation 1	**ATG**TTTGTGTTGAAATCAGTGGTGCTCTGTGCG.*CTGGAGCCCAGTCGTGCCCGTCCCAGTGCT*	DELETION - 13 nucleotides
slit2 mutation 2	**ATG**TTTGTGTTGAAATCAGTGGTGCTCTGTGC.*GGGGCTGGAGCCCAGTCGTGCCCGTCCCA*	DELETION - 10 nucleotides
slit2 mutation 3	**ATG**TTTGTGTTGAAATCAGTGGTGCTCTGTGCG TTGC.*GGGGCTGGAGCCCAGTCGTGCCCGT*	DELETION - 5 nucleotides
slit2 mutation 4	**ATG**TTTGTGTTGAAATCAGTGGTGCTCTGTGCG TTGCT.*T.CTGCGGGGCTGGAGCCCAGTCGT*	INSERTION - 1 nucleotide

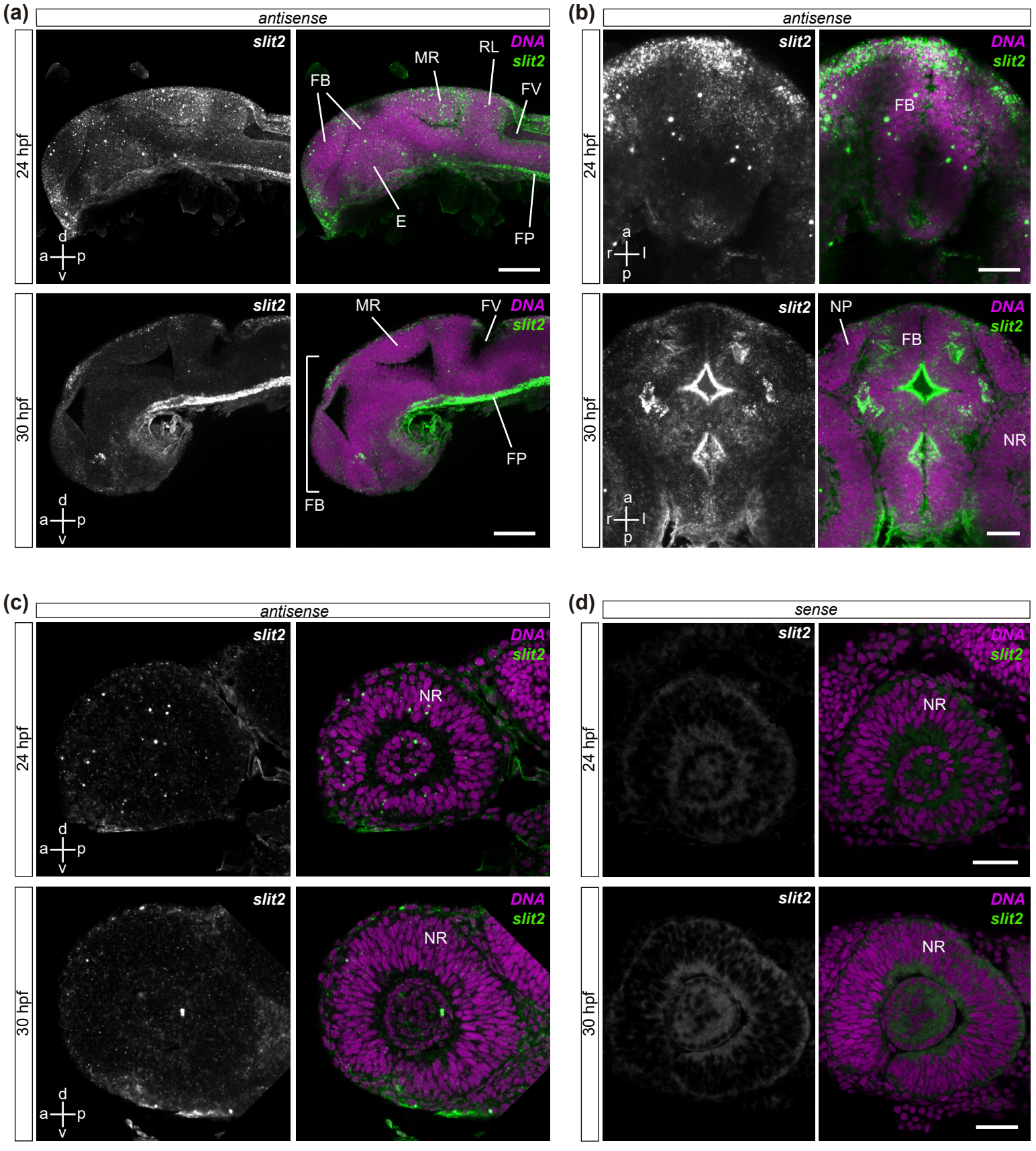
(a)
antisense
24 hpf
slit2
DNA
slit2
MR
RL
FB
FV
E
FP
d
a
p
v
30 hpf
slit2
DNA
slit2
MR
FV
FP
FB
d
a
p
v
(b)
antisense
24 hpf
slit2
DNA
slit2
FB
a
r
l
p
30 hpf
slit2
NP
DNA
slit2
FB
NR
a
r
l
p
(c)
antisense
24 hpf
slit2
DNA
slit2
NR
d
a
p
v
30 hpf
slit2
DNA
slit2
NR
d
a
p
v
(d)
sense
24 hpf
slit2
DNA
slit2
NR
30 hpf
slit2
DNA
slit2
NR

Suppl. Fig. 2

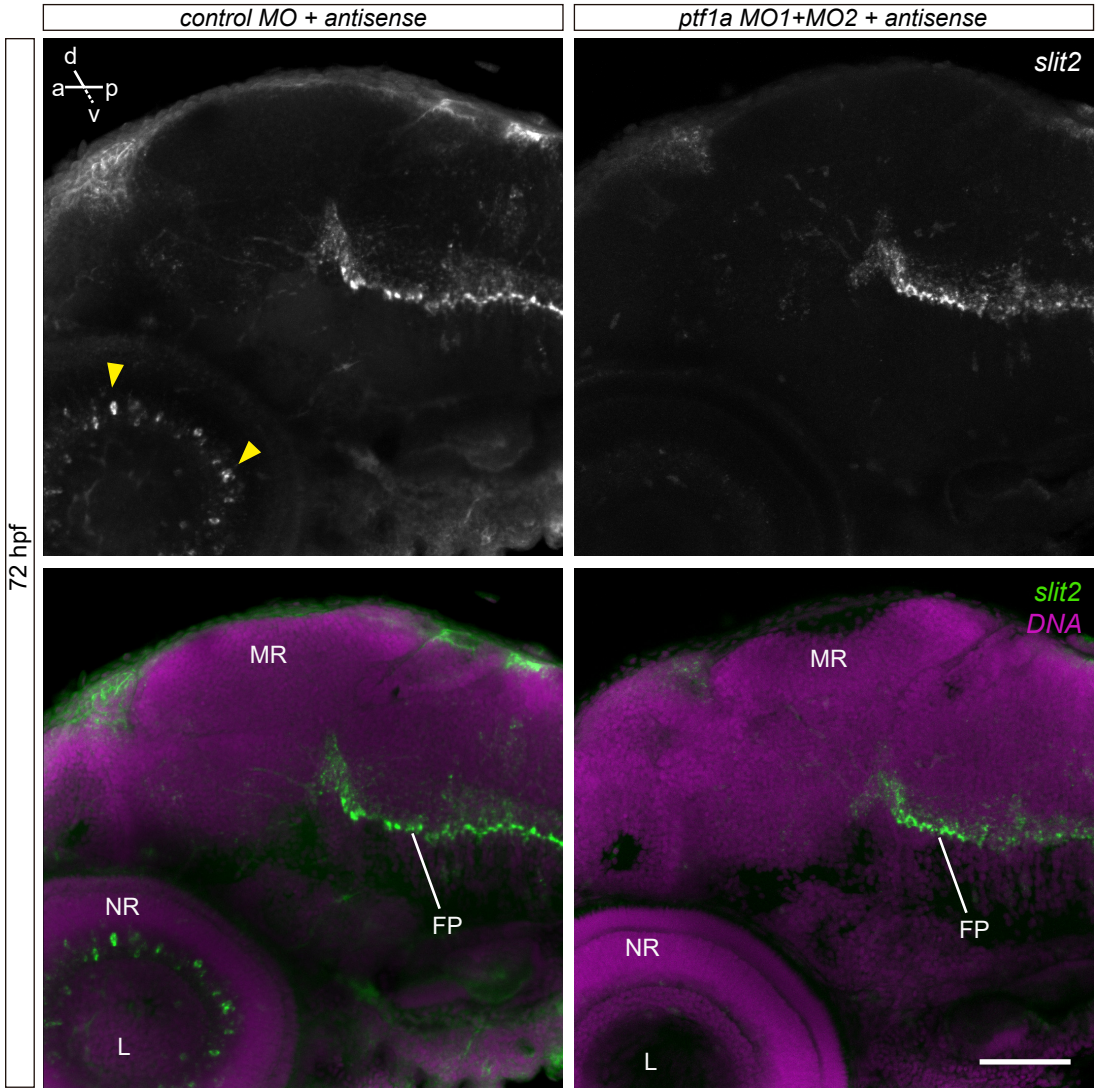
control MO + antisense
ptf1a MO1+MO2 + antisense
72 hpf
d
a
p
v
slit2
MR
NR
L
FP
slit2
DNA

Suppl. Fig. 3

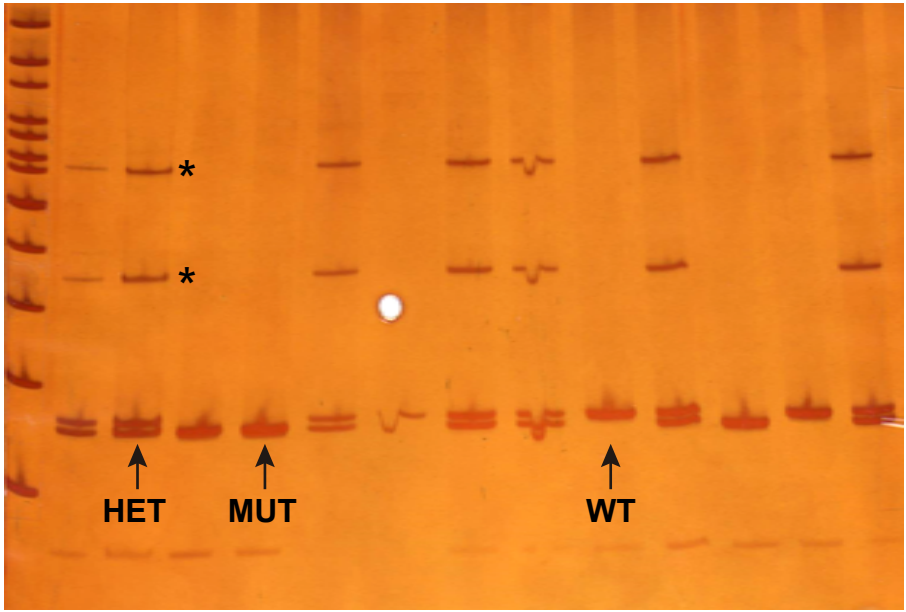

Suppl. Fig. 4

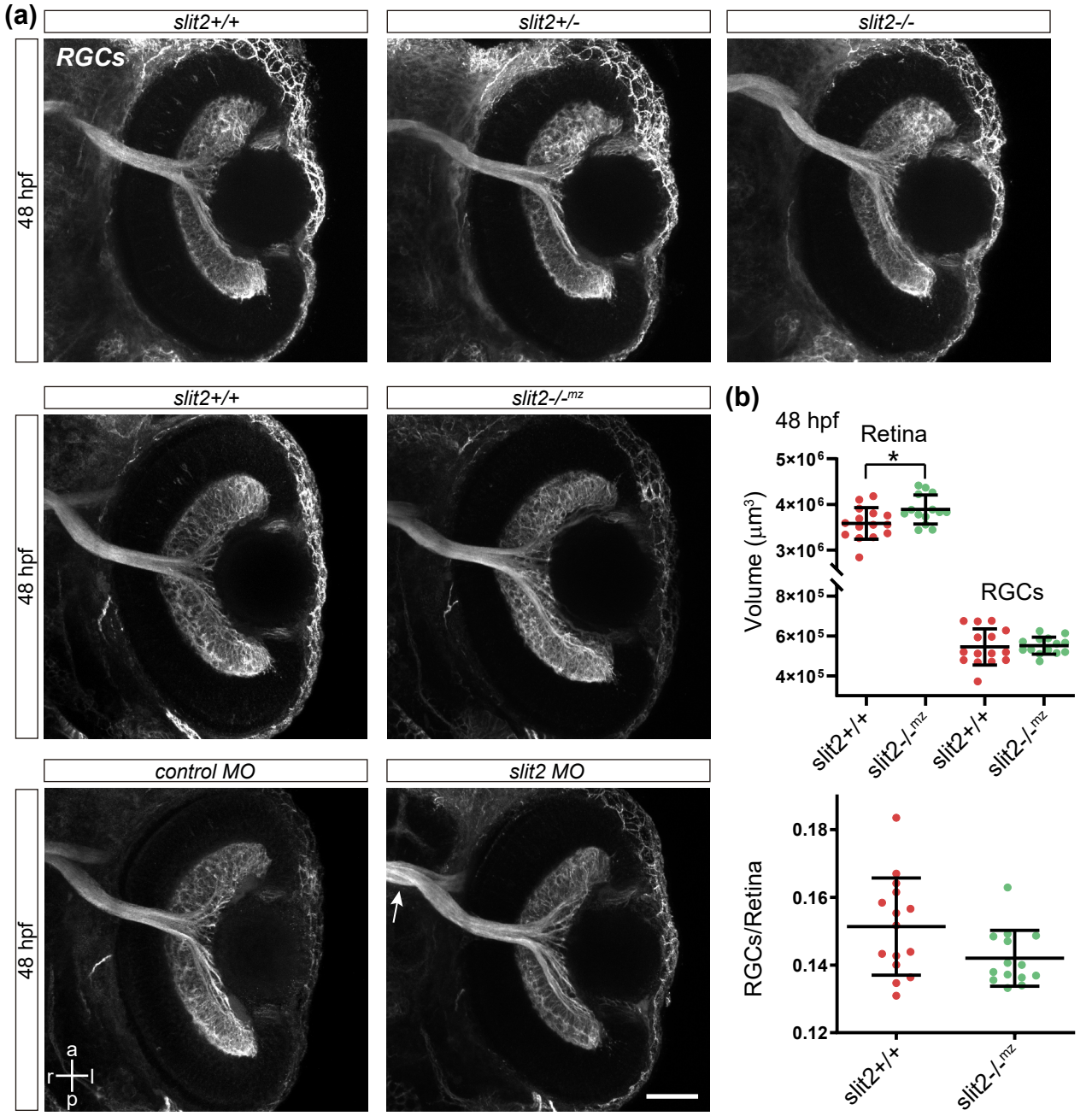
(a)
slit2+/+
slit2+/-
slit2-/-
RGCs
48 hpf
slit2+/+
slit2-/-mz
48 hpf
control MO
slit2 MO
48 hpf
a
r
l
p
(b)
48 hpf
Retina
RGCs
*
Volume (µm3)
5×10^6
4×10^6
3×10^6
8×10^5
6×10^5
4×10^5
slit2+/+
slit2-/-mz
slit2+/+
slit2-/-mz
RGCs/Retina
0.18
0.16
0.14
0.12
slit2+/+
slit2-/-mz

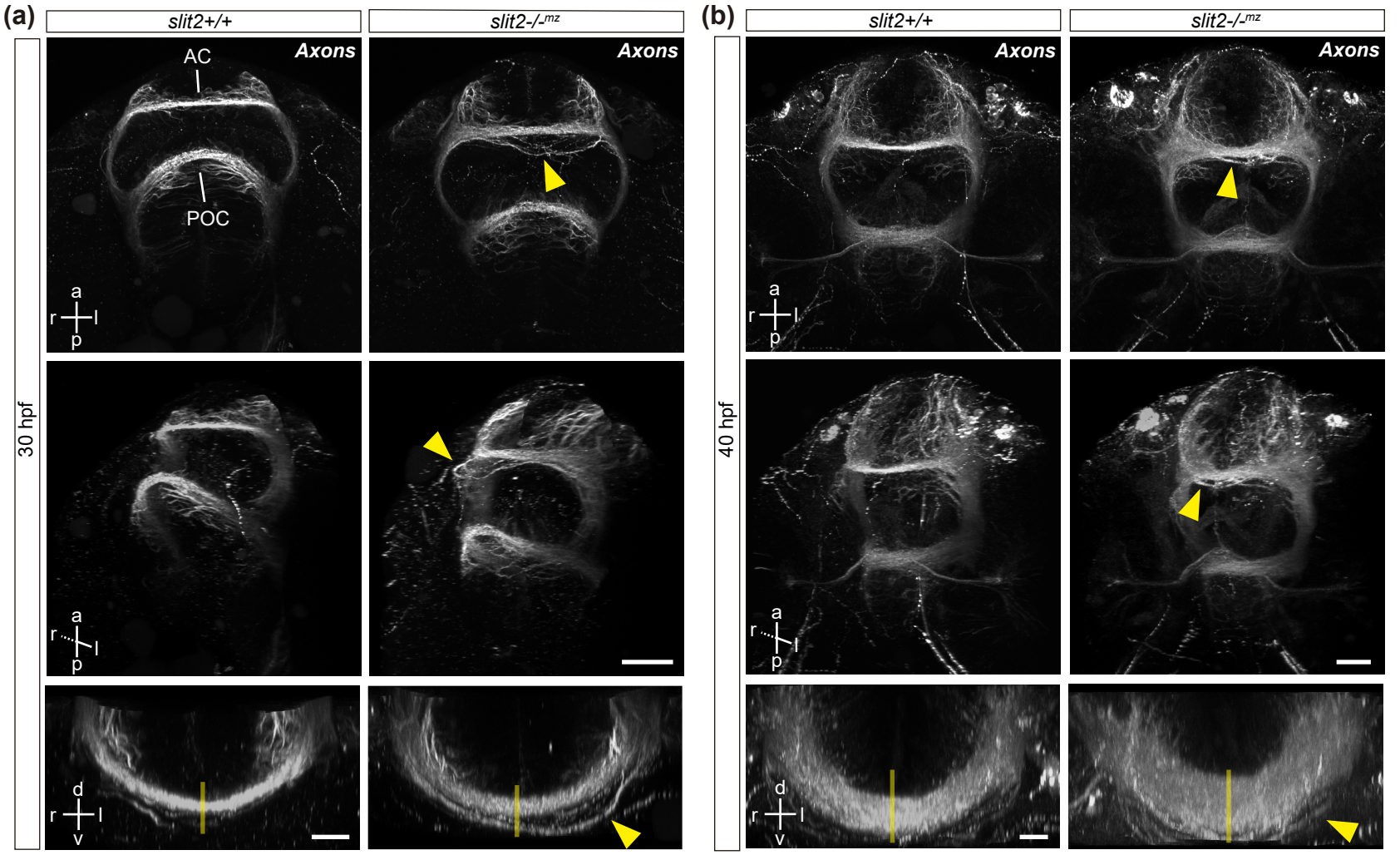
(a)
slit2+/+
slit2-/-mz
30 hpf
Axons
AC
POC
(b)
40 hpf
(c)
30 hpf
slit2+/+
slit2-/-mz
Fluorescence intensity (UA)
Distance (µm)
40 hpf

Suppl. Fig. 6